Metabolic syndrome in New Zealand Obese mice promotes microglial-vascular interactions and reduces microglial plasticity

Michael MacLean[1], Olivia J. Marola[1], Travis Cossette[1], Cory Diemler[1], Amanda A. Hewes[1], Kelly J. Keezer[1], Kristen D. Onos[1*], and Gareth R. Howell[1,2,3*]

[1]The Jackson Laboratory, Bar Harbor, ME 04609, USA

[2]Sackler School of Graduate Biomedical Sciences, Tufts University School of Medicine, Boston, MA 02111, USA

[3]Graduate School of Biomedical Sciences and Engineering, University of Maine, Orono, ME 04469, USA

Correspondence:[*] gareth.howell@jax.org and kristen.onos@jax.org

Summary:

Metabolic syndrome (MetS) puts patients more at risk for neurodegenerative diseases such as Alzheimer's disease (AD). Microglia are implicated as causal factors in AD, however, the effect of MetS on microglia has not been characterized. To address this, we contrasted New Zealand Obese (NZO) with C57BL/6J (B6J) mice in combination with a high fat/high sugar diet (HFD). Irrespective of diet, NZO mice displayed a broader array of MetS-relevant phenotypes compared to B6J mice fed a HFD. Single cell RNA-sequencing of microglia predicted transcriptional shifts indicative of reduced responsiveness and increased vascular interactions in NZO, but not B6J HFD mice. Significant cerebrovascular fibrin deposition and increased perivascular accumulation of microglia were observed in NZO relative to B6J HFD mice. Further, compared to the widely used B6J.*APP/PS1* mice, NZO.*APP/PS1* exhibited increased amyloid plaque sizes alongside an increase in microhemorrhages. Overall, our work supports a model whereby MetS alters microglia-vascular interactions, compromising microglial plasticity.

Introduction:

Metabolic syndrome (MetS) is a combination of three or more metabolic impairments such as dyslipidemia, hyperglycemia, hypertension, and increased waist circumference (1). Patients displaying aspects of MetS are more at risk for neurodegenerative disorders including Alzheimer's disease (AD) (2-6). Central to this risk may be the influence of MetS and Type 2 Diabetes (T2D) on peripheral and central immune cell states and function (7,8).

Burgeoning evidence has implicated critical roles for microglia, central nervous system (CNS) resident macrophages, in neurodegeneration (9-15). Microglia play roles in pathogen surveillance, debris phagocytosis, synapse regulation, and recently have been shown to support the cerebral vasculature (16-21). Current efforts have uncovered remarkable heterogeneity of microglial responses through single cell RNA-sequencing (scRNA-seq) (9,11,15,22). Increased disease-associated microglia (DAM) (11,12) and interferon response microglia (IRM) states (23) have been documented in neurodegeneration. The abundance of these states is heavily dependent on additional factors including age, sex, and genetic context (15,22-25). However, the effect of MetS on microglial states has yet to be determined.

To address this, we investigated MetS-induced changes in microglial transcriptional states using scRNA-seq. We utilized combinations of genetic and environmental models relevant to MetS contrasting New Zealand Obese (NZO/HlLtJ) mice, a polygenic model of obesity (26-28), with the commonly used C57BL/6J (B6J) mice fed a high fat/high sugar diet (HFD). Microglia scRNA-seq suggested MetS resulted in reduced microglial responsiveness in NZO mice relating to vascular

interactions and function. In support of this, NZO but not B6J mice exhibited fibrin deposition within the cerebrovasculature. NZO mice also showed reduced microglia responses to an acute lipopolysaccharide (LPS) challenge compared to B6J mice, and larger amyloid-β plaques and increased microhemorrhages in the presence of *APP/PS1* transgenes (NZO.*APP/PS1*) compared to B6J.*APP/PS1* mice. In summary, MetS appeared to impair microglial plasticity, which could potentially drive neurodegenerative disease pathology.

Results:

Metabolic syndrome (MetS) caused subtle changes in abundances of microglia states.

To determine how MetS affects microglia, we fed NZO and B6J mice a HFD or a standard diet (SD) from 2-9 months of age (mo). NZO mice showed signs of MetS at 2mo (Figure 1A-E). At 9mo, NZO mice displayed increased age- and diet-associated metabolic impairments relative to B6J mice, including weight gain, dyslipidemia, high blood pressure, and hyperglycemia (Figure 1F-J). These data indicate that the NZO strain better models complex endophenotypes observed in humans with MetS compared to HFD-fed B6J mice.

To determine the effects of strain (NZO, B6J) and diet (SD, HFD) on myeloid cell transcriptional states, we performed scRNA-seq of $CD11B^{+}$ cells (24,29) from brains of 2 and 9mo male and female B6J, B6J HFD, NZO, and NZO HFD mice (Figure 2A). Microglia represented ~75% of all captured $CD11B^{+}$ cells in B6J mice, and ~88% in NZO mice, irrespective of diet (Figure S1A-D) (30,31). The remaining cells consisted mainly of monocytes, macrophages, NK cells, and neutrophils (Figure S1D). Re-

clustering only microglia resulted in 18 clusters (Figure S1E-F) with further annotation as: homeostatic (H, clusters: 0-6,9, 13,14, and 16), proliferating (cluster 17), *Hexb* high (HexB, cluster 10), disease-associated (DAM, cluster 8), *Ccl4 Ccl3* high DAM (*Ccl4*$^{+}$ *Ccl3*$^{+}$ DAM, cluster 7), major histocompatibility enriched (MHC, cluster 16), interferon responsive microglia (IRM, cluster 12) and *Klf2 Tcim* high (*Klf2*$^{+}$ *Tcim*$^{+}$, cluster 13) (Figure 2B-D, Figure S1E-F) (11,12,22,24). In contrast to amyloid- (11,12,24) and aging-related (22) studies, MetS (NZO strain and/or HFD) did not cause significant changes in the percentages of DAM, IRM or MHC clusters (Figures 2E, S2A). However, the abundance of DAM, MHC, and *Klf2*$^{+}$ microglia changed with age, regardless of strain or diet (Figure 2E, Figure S2A-B).

High fat diet altered stress response and cell-cell communication gene expression in NZO, but not B6J microglia.

Despite the lack of MetS-induced shifts in microglial states (Figure 2E), we reasoned that MetS may alter gene expression across all microglia. To determine this, we utilized a pseudobulking strategy followed by differential expression analyses, separately assessing the strain (NZOvB6J), and diet (HFDvSD) or aging (9v2mo) effect within each strain (Figure S3A-B)(32,33). First, we determined the HFD effect across both NZO and B6J mice and found that there were 141 differentially expressed genes (DEGs) in all microglia, which were enriched in gene sets associated with cell viability, migration, and proliferation (Figures 3A, S4A-C). However, when HFD effects were analyzed separately for each strain, B6J microglia did not show a substantial response to chronic HFD exhibiting only 2 DEGs in comparison with >300 DEGs in NZO microglia (Figure

3A,S4D). These NZO DEGs were associated with endothelial and immune cell signaling, and heat shock stress (Figure 3B-D). Together, these data suggest HFD caused a significant stress response in microglia in NZO, but not B6J mice.

Aging differentially effected NZO and B6J microglia.

To assess transcriptional programs in NZO compared to B6J, we first identified DEGs comparing NZO to B6J microglia at 2 or 9mo. DEGs identified at both ages included genes that have been implicated in regulating microglial and macrophage responses, such as *Angptl7*, *Itgam,* and *Fcrls* (Figure 4A-B,S5A-D) (22,34-36). Interestingly, *Apoe*, genetic variations in *APOE* increase risk for AD (37,38), was significantly greater in NZO compared to B6J microglia at both ages (Figure 4C). At 9mo, DEGs were associated with immune responses, vascular interactions, and cell migration (Figure 4D-E), suggesting these processes are perturbed in NZO but not B6 microglia. When microglia states were analyzed separately, differentially expressed genes detected in all microglia were primarily driven by homeostatic microglia, downsampling indicated this was independent of the number of microglia within each state (Figure S5A-B).

Next, to better understand how transcriptional programs were influenced by aging, we compared 9 to 2mo microglia from either NZO or B6J mice (Figure 4F). Most aging related transcriptional changes were again detected within the homeostatic microglia state when analyzed separately (Figure S6A-B). Both strains showed aging-associated changes in *Itga6*, *Ctss*, *Cd48*, and antigen processing and presentation pathways (Figure 4F-I). However, NZO microglia exhibited more aging-associated

DEGs than B6J including *Sparc*, *Pfkfb3,* and *Irf8*; which have been implicated in regulating synaptic function, glycolysis, and microglial identity respectively (Figure 4F-G) (39-41). In addition, NZO microglia exhibited age-dependent changes in cytotoxicity, wound healing, and circulation pathways (Figure 4I). Interestingly, Ingenuity Pathway Analysis (IPA) of upstream regulators predicted aging-associated upregulation of interferon signaling regulators in B6J microglia, but regulators associated with environmental stress and tissue repair in NZO microglia (Figure S6C-E).

NZO microglia displayed increased association with blood vessels.

The expression of genes regulating myeloid-endothelial interactions including *Itgam*, *Ccr1, P2ry12*, and *Ccr5* (16,35,36,42), was higher in NZO relative to B6J microglia (Figure 4). To probe this further, we performed immunohistochemistry to localize microglia and vasculature within the cortex and hippocampus of 9mo NZO and B6J mice fed SD or HFD. We found that while the numbers of $TMEM119^{+}DAPI^{+}$ microglia in the hippocampus or cortex did not differ across strains or diets, the percentage of $CD31^{+}$ area covered by microglia was significantly higher in NZO relative to B6J mice (Figure 5A-E). HFD did not modulate this phenomenon (Figure 5B-E). scRNA-seq analyses predicted fibrin(ogen) to be an upstream regulator of aging-associated DEGs in NZO microglia (Figure 5F). Fibrin is absent in the healthy CNS but can deposit in the perivascular space and within vessels in conditions of stress (38,43,44). We found NZO vessels exhibited peri-vascular and vascular deposition of fibrin in the hippocampus and cortex, while B6J vessels did not (Figure 5G-I). Furthermore, many of these $fibrin^{+}$ vessels had microglia juxtaposed (Figure 5G).

Altogether, these data suggest that vessel stress signals may promote microglia-vascular interactions in NZO mice.

NZO mice displayed a dampened response to LPS.

As NZO microglia appeared to have a reduction in DEGs relevant to immune responses compared to B6J microglia (Figure 4,S5), we sought to probe the responsiveness of NZO microglia to an acute inflammatory challenge. LPS was administered to 4mo NZO and B6J mice, and bulk hemibrain RNA-seq (Figure 6A) was performed. As we suspected from the observed fibrin deposition, NZO animals exhibited altered CNS expression of vascular associated pathways and genes including *Edn1, Angpt1,* and *Serpine1* (Figure 6B-C) even with PBS-treatment. LPS-treated NZO animals also displayed fewer DEGs than LPS-treated B6J mice (Figure 6D). The strain-dependent LPS effects suggested potential differences in microglial responses, as NZO animals displayed no change in *Cx3cr1* expression with LPS treatment (Figure 6E). Furthermore, IPA upstream regulator and pathway analyses predicted strain-dependent differences in the LPS induction of genes involving macrophage recruitment, antigen processing and presentation, and aggregation of cells (Figure 6F). These data indicate that compared to B6J, NZO mice display altered microglial responses to not only HFD, but also to an acute insult such as LPS.

NZO.APP/PS1 mice displayed larger amyloid plaques and increased incidences of microhemorrhages.

MetS has been demonstrated to increase risk for AD and related dementias (2,4,5,45). We hypothesized that this may be due to reduced responsiveness of microglia to AD-relevant insults such as amyloid deposition. To test this, we backcrossed the commonly used amyloid-inducing transgenes (*APP/PS1*) (46) from B6J to NZO resulting in ~98.375% congenicity. Unexpectedly, male NZO.*APP/PS1* mice exhibited pronounced weight loss, likely associated with exacerbation of T2D (Figure S7A-E). To avoid this confound, we primarily focused our analyses on amyloid-related microglia responses in female mice. At 8mo, in comparison to B6J.*APP/PS1* mice, female NZO.*APP/PS1* mice exhibited fewer, but larger, amyloid plaques in both the hippocampus and cortex, which were positive for the dystrophic neurite marker LAMP1 (Figure 7A-L). Similar results were observed in several male NZO.*APP/PS1* mice that survived to 8mo (Figure S7F-G). There was a small but significant increase in total $IBA1^+$ area in the hippocampus, but not the cortex of NZO.*APP/PS1* compared to B6J.*APP/PS1* mice (Figure 7F,K). However, the area of plaque covered by microglia were the same in both regions (Figure 7G, L).

Previous studies have shown microglia depletion drives development of cerebral amyloid angiopathy (CAA) (14,47). We wondered whether the reduced responsiveness of NZO microglia would result in increased CAA. However, extensive CAA was not present in NZO.*APP/PS1* or B6J.*APP/PS1* mice (Figure 7A, S7F-G). Our previous findings of increased vascular stress in NZO (Figures 5-6) suggested blood-brain-barrier integrity may be more compromised in NZO.*APP/PS1* compared to B6J.*APP/PS1* mice. To assess this, we stained brain tissue with Prussian blue, which marks areas of iron deposition, and found that NZO.*APP/PS1* mice displayed increased incidence of

microhemorrhages throughout the brain relative to either B6J.*APP/PS1* mice or their WT littermate controls (Figure 7M-N).

Together, these data support that in a context of MetS, amyloid plaques are larger and the cerebrovasculature is more prone to microhemorrhages, outcomes which may increase risk for diseases such as AD.

Discussion:

Our work focused on the relationship between MetS and alterations in microglial responses using mice exhibiting varying aspects of MetS (26-28). Consistent with previous reports, NZO mice displayed most aspects of MetS, and this was exacerbated with HFD. However, HFD-fed B6J mice exhibited dysfunctional metabolic measures associated only with pre-diabetes and obesity, identifying NZO mice as a more appropriate model of MetS than B6J HFD mice. We profiled 83,757 microglia and unexpectedly, MetS did not significantly shift the proportion of previously identified microglial states (11,12,22,24). We noted an increase in MHC and *Klf2*$^{+}$ transcriptional states and a decrease in both DAM populations between 2 and 9mo. This is consistent with previous reports of age-related alterations in MHC and DAM microglia populations (48).

We identified significant strain-specific changes in gene expression programs across all microglia, and within specific states. Strikingly, when we analyzed differential expression within each state, cells within the homeostatic clusters exhibited the greatest number of DEGs even after downsampling. This suggests that these transcriptional changes, while not sufficient to alter state abundances, are potentially altering microglial

function. Strain-specific differences in microglia are likely driven by the MetS endophenotypes exhibited by NZO as early as 2mo. NZO microglia exhibited significantly higher expression of *Apoe* compared to B6J or B6J HFD microglia. ApoE has been linked to the transition to a DAM (or activated response microglia) state (12,23), yet, there was no difference in the abundance of DAM between NZO and B6J mice. One explanation for this paradox may be that the increase in *Apoe* expression is in response to dyslipidemia, as ApoE has known roles in lipid metabolism (37,49,50). Furthermore, it is possible that NZO microglia are unable to fully transition to a DAM state yet still acquire DAM-like characteristics such as high *Apoe* expression. In addition to the aging- and HFD-independent strain differences, there were also significant aging- and HFD-dependent strain differences between NZO and B6J microglia. For instance, aging influenced NZO microglia more than B6J microglia through higher numbers of DEGs and a broader range of impacted pathways, including wound healing and cytotoxicity. One recent study suggested that NZO mice display enhanced aging-associated changes within peripheral immune populations —suggesting that NZO were a model of accelerated aging (51) — and our data also support this possibility.

A prevailing signature of both aging- and strain-associated analyses implicated microglia differential interactions with the vasculature. Further exploration through IHC highlighted that regardless of diet, NZO mice exhibited more perivascular microglia than B6J mice. Upstream regulator analysis predicted fibrin may a significant culprit behind aging-associated changes in NZO microglia and fibrin deposition was detected in NZO brains. Fibrin has previously been shown to be neurotoxic (35,36). Fibrin upregulates *Hmox1* expression in microglia (36) and upstream regulator analysis predicted

activation of HMOX1-dependent inflammatory response signaling pathways when comparing 9mo NZO and B6J microglia. Furthermore, MetS has been associated with increased CCL5, which can recruit immune cells via CCR1/CCR5 to vasculature (52-54). NZO mice exhibit peripheral vascular stress (55), and NZO microglia display higher expression of *Ccr1* and *Ccr5*.

Collectively, these data predict MetS may increase vascular stress and fibrin deposition in the CNS, resulting in recruitment of microglia to the cerebrovasculature. This primary endophenotype may than render microglia less responsive to a secondary insult. To test this, we first used an acute LPS treatment and performed bulk RNA-seq on hemibrains. We found increased expression of vascular associated genes in NZO hemibrains relative to B6J hemibrains including *Serpine1*, *Edn1* and *Angpt1* which mediate vascular stress and fibrin accumulation (56-58). Further, fewer DEGs were identified in LPS-treated NZO mice compared to LPS-treated B6J. This provides support for decreased responsiveness in NZO microglia. For example, *Cx3cr1* did not change in LPS-treated NZO mice. *Cx3cr1* expression has been shown to decrease in neurodegeneration (11,12). Interestingly, recently published data suggest aged microglia display a dampened response to LPS, supporting the concept that NZO mice may be a model of MetS-dependent accelerated aging (59).

Following acute stimuli, we turned to a more chronic and disease-relevant inflammatory stimulus, amyloid deposition (12,14,23,60). We found that NZO*.APP/PS1* mice displayed a significant increase in plaque size, independent of numbers of plaque-associated microglia. Increased plaque sizes may impact larger regions leading to increased likelihood of cognitive dysfunction. Patients displaying MetS have accelerated

plaque deposition, and MetS blood biomarkers correlate with the rate of cognitive decline in patients with MCI and dementia (61,62). One possibility for the increased plaque size is in NZO.*APP/PS1* compared to B6J.*APP/PS1* mice is inefficient plaque compaction or clearance by NZO microglia - that would fit with the model of MetS-dependent reduced responsiveness. A second possibility may be altered activity of insulin degrading enzyme (IDE). In addition to insulin degradation, IDE also contributes to plaque degradation (63). Microglia-specific or brain-wide *Ide* expression was not changed between NZO and B6J mice, however, a MetS-dependent increase in insulin, requiring degrading by IDE in NZO mice, may result in reduced amyloid-β degradation.

Emerging work has implicated microglia in regulating blood flow and closure of injured vascular barriers (16,18,64). Therefore, given the vascular stress and changes to microglia-vascular interactions in NZO mice, we investigated whether NZO.*APP/PS1* mice were susceptible to microhemorrhages. NZO.*APP/PS1* mice presented with microhemorrhages, which were rare in B6J.*APP/PS1* mice or WT littermate controls. Microhemorrhages are more common in AD patients than in control groups and were previously detected in *Ob/Ob APP/PS1* mice (65-68). One possible mechanism driving the microhemorrhages in NZO.*APP/PS1* mice relates to fibrin deposition. Fibrin is stabilized by amyloid-β potentiating vascular damage and blood-brain-barrier breakdown (38,69). Recent evidence suggests the amount of fibrin coverage of vessels correlates to cerebral microbleeds in patients with CAA (70). Yet, we did not observe extensive CAA in NZO.*APP/PS1* mice. It is possible microhemorrhages in NZO.*APP/PS1* mice are a result of the inability of microglia to clear fibrin and/or amyloid-β efficiently, alongside potential impairments in wound healing and vascular

repair pathways may predispose NZO mice to increased microhemorrhages. Diabetes worsens wound healing and vascular repair pathways in a variety of pathological conditions (71) and NZO microglia exhibit age-associated alterations in wound healing pathways underscoring this possibility. These data provide further evidence that MetS reduces or dampens the responsiveness of microglia.

In summary, we have found that MetS in NZO mice fundamentally altered microglia responses even when compared to microglia of HFD-fed B6J mice. NZO microglia displayed age-associated transcriptional changes concomitant with increased perivascular association. These changes were associated with abnormal responses to an acute LPS challenge and chronic amyloid pathology altogether suggesting MetS reduced microglial plasticity. Overall, this also supported the hypothesis of accelerated aging in NZO compared to B6J. This work provides the foundation to investigate the mechanisms by which MetS compromises microglial responses, leading to increased risk for neurodegenerative disease such as Alzheimer's disease.

Acknowledgments:

We gratefully acknowledge the contribution of the Single Cell Biology Laboratory, Clinical Chemistry and Genomic Technologies Cores at The Jackson Laboratory (JAX) for expert assistance with this publication. We thank Dan Skelly from JAX Computational Sciences for advice on single-nucleotide polymorphisms based demultiplexing of scRNA-seq data. We thank Bansri Patel from the JAX Summer Student Program and Matthew Cox, a Mount Desert Island High School student intern, for preliminary investigations into NZO.*APP/PS1* animals.

This study was supported in part by National Institutes of Health National Institute of Aging T32G062409A (M.M.), JAX Scholars Program (M.M.); The Jackson Laboratory startup funds (G.R.H.), a BrightFocus Foundation award G2020254 (G.R.H.), and ongoing philanthropic support from the Diana Davis Spencer Foundation and other anonymous donors (G.R.H.). G.R.H holds the Diana Davis Spencer Foundation chair for glaucoma research. The funders had no role in study design, data collection, analysis, decision to publish, or preparation of the manuscript.

Author contributions:

M.M, K.D.O., and G.R.H. designed the study. M.M. developed experimental protocols, completed *in vivo* and IHC experiments and analyses, performed microglia isolations, and scRNA-seq bioinformatics analyses. O.J.M, C.D., T.C., K.D.O. and K.J.K, and A.A.H., all contributed to experiments. A.H., M.M., and K.J.K. generated and maintained mice for this study. M.M, K.D.O., and G.R.H. wrote the manuscript. All authors approved the final version.

Declaration of interests:

The authors declare no competing interests.

Figure Legends:

Figure 1. Strain-dependent effects of both high-fat diet and aging on characteristics of metabolic syndrome.

a. Body weight at 2mo. **b.** Fasted cholesterol at 2mo. **c.** Fasted triglycerides at 2mo. **d.** Hemoglobin A1c (HbA1c) at 2mo. **e.** Blood pressure at 2mo. **f.** Body weight of mice fed either SD or HFD from 2-9mo. **g.** Fasted cholesterol at 9mo. **h.** Fasted triglycerides at 9mo. **i.** HbA1c at 9mo. **j.** Blood pressure at 8mo. In **a**–**e**: two-way ANOVA with post-hoc Tukey's test. In **a,** *N*=16 NZO (7M,9F), *N*=23 B6J (11M,12F) mice. In **b-c**, *N*=7 NZO (4M,3F), *N*=8 B6J (4M,4F) mice. In **d**, *N*=8 NZO (4/sex), *N*=9 B6J (4M,5F) mice. In **e**, *N*=4M mice/strain. In **f**, mixed effects model with repeated measures. *N*=7M NZO (4SD,3HFD), *N*=9F NZO (4SD,5HFD), *N*=11M B6J (5SD,6HFD), *N*=12F B6J (7SD,5HFD). In **g-h**, *N*=7M NZO (4SD,3HFD), *N*=9F NZO (4SD,5HFD), *N*=10M B6J (5SD,5HFD), *N*=12F B6J (7SD,5HFD). Dashed lines and represent values > 200mg/dL. In **i**, *N*=7M NZO (4SD,3HFD), *N*=9F NZO (4SD,5HFD), *N*=10M B6J (4SD,6HFD), *N*=11F B6J (6SD,5HFD). Red line indicates diabetic HbA1c, gray line indicates prediabetes. In **j**, *N*=13M NZO, *N*=9M B6J mice. All data shown are Mean±SEM.

Figure 2. Profiling myeloid transcriptional states in a cohort of varying metabolic impairment.

a. Experimental design scheme; created with BioRender.com. **b.** Dimensionality reduction plot (UMAP) of microglia colored by cluster. **c.** UMAPs of microglia colored by SCT-normalized expression of marker genes. **d.** Dot plot of marker genes associated with each annotated state. **e.** UMAP of microglia colored by annotated state. In **a-e**, 9mo mice: *N*=3M NZO/diet, *N*=4F NZO/diet, *N*=4M B6J/diet, *N*=3F B6J/diet; 2mo mice: *N*=3 NZO/sex, *N*=7 B6J (3M,4F).

Figure 3. HFD promotes stress-responses and alters cellular communication pathways in NZO but not B6J microglia.

a. Bar chart summarizing the number of DEGs associated with HFDvSD across all microglia, within NZO microglia alone, and within B6J microglia alone. **b.** IPA graphical summary of NZO HFDvSD microglia DEGs. **c.** Violin plots of selected HFDvSD NZO DEGs. **d.** Enrichment GO term plot for NZO HFDvSD microglia DEGs. In **a-d**, *N*=3M NZO/diet, *N*=4F NZO/diet, *N*=4M B6J/diet, *N*=3F B6J/diet mice.

Figure 4. NZO and B6J microglia exhibit strain- and age- associated transcriptional differences.

a. Venn diagram displaying overlap of NZOvB6J DEGs at 2 and 9mo. **b.** Violin plots of a subset of NZOvB6J 9mo DEGs. **c.** UMAP plots for NZO and B6J microglia. Colored by SCT-normalized *Apoe* expression. **d.** Enrichment GO term plot of 9mo NZOvB6J microglia DEGs. **e.** IPA graphical summary of 9mo NZOvB6J DEGs. **f.** Venn diagram of 9v2mo DEGs identified in NZO and B6J microglia. **g.** Violin plots of selected 9v2mo NZO microglia DEGs. Enrichment GO term plots for 9v2mo B6J (**h**) or NZO (**i**) microglia DEGs. 9mo mice: *N*=7 NZO (3M,4F), *N*=7 B6J (4M,3F). 2mo mice: *N*=6 NZO mice (3M,3F), *N*=7 (3M,4F) B6J mice.

Figure 5. NZO vasculature displays fibrin deposition concomitant with increased coverage by microglia.

a. Representative images of TMEM119 and CD31 staining in the hippocampus. Quantification of microglia in the hippocampus (**b)** and cortex (**d**). Quantification of the

percentage of CD31 colocalized with TMEM119 in the hippocampus (**c**) and cortex (**e**). **f.** IPA upstream regulator analysis of 9v2mo NZO microglia DEGs. **g.** Representative images of TMEM119, CD31, and fibrin. Insets are high resolution confocal imaging of noted area. Quantification of the percentage of CD31 colocalized with fibrin in the hippocampus (**h**) and cortex (**i**). *N*=8 NZO (2/sex/diet) and *N*=8 B6J (2/sex/diet) mice. In **b**-**c**, independent two sample two-sided *t* test. In **e**, **h-i**, Mann-Whitney test. SD: closed circles, HFD: open circles. Data are presented as Mean±SEM.

Figure 6. NZO animals display increased expression of hemibrain vascular associated genes and an altered central nervous system response to an acute LPS treatment.
a. Experimental schematic of CNS responsiveness to LPS. Created with BioRender.com. **b.** Bar chart of DEGs associated with each comparison. **c.** Top IPA regulatory effect for NZOvB6J DEGs. **d.** Venn diagram displaying DEGs associated with the LPS response in each strain. **e.** Volcano plot of the Strain-by-Treatment interaction effect. Top 10 genes by significance are labeled. Genes are colored by significance. **f.** IPA graphical summary of the Strain:LPS interaction effect. In **a-f**, N=3F mice/strain/treatment.

Figure 7. NZO mice exhibit fewer, but larger neuritic amyloid plaques, without differences in microglia coverage of plaques.
Representative images of 6E10 amyloid-β staining with IBA1 (**a**) or regions of interest with LAMP1 co-staining (**b**) in the hippocampus. **c.** Quantification of $6E10^{+}$ area in the hippocampus (**c**) and cortex (**h**). Quantification of $6E10^{+}$ counts in the hippocampus (**d**)

and cortex (**i**). Quantification of the average size of 6E10$^+$ objects in the hippocampus (**e**) and cortex (**j**). Quantification of IBA1$^+$ area in the hippocampus (**f**) and cortex (**k**). Quantification of the percentage of 6E10$^+$ area colocalized with IBA1$^+$ area in the hippocampus (**g**) and cortex (**l**). **m**. Representative images of Prussian blue staining with higher magnification image of the inset. **n.** Quantification of Prussian blue$^+$ microhemorrhages per brain section. SD: closed circles, HFD: open circles. In **a-l**, *N*=4F NZO.*APP/PS1*, *N*=3F B6J.*APP/PS1* mice. Independent two sample two-sided *t* test. In **m-n**, *N*=4/strain/diet WT mice and *N*=4F NZO, *N*=3F B6J *APP/PS1* mice. Two-way ANOVA with post-hoc Tukey's test. Data are presented as Mean±SEM.

1. Lam, D. W., and LeRoith, D. (2000) Metabolic Syndrome. in *Endotext* (Feingold, K. R., Anawalt, B., Blackman, M. R., Boyce, A., Chrousos, G., Corpas, E., de Herder, W. W., Dhatariya, K., Dungan, K., Hofland, J., Kalra, S., Kaltsas, G., Kapoor, N., Koch, C., Kopp, P., Korbonits, M., Kovacs, C. S., Kuohung, W., Laferrere, B., Levy, M., McGee, E. A., McLachlan, R., New, M., Purnell, J., Sahay, R., Shah, A. S., Singer, F., Sperling, M. A., Stratakis, C. A., Trence, D. L., and Wilson, D. P. eds.), South Dartmouth (MA). pp
2. Kim, Y. J., Kim, S. M., Jeong, D. H., Lee, S. K., Ahn, M. E., and Ryu, O. H. (2021) Associations between metabolic syndrome and type of dementia: analysis based on the National Health Insurance Service database of Gangwon province in South Korea. *Diabetol Metab Syndr* **13**, 4
3. Karaca, C., and Karaca, Z. (2018) Beyond Hyperglycemia, Evidence for Retinal Neurodegeneration in Metabolic Syndrome. *Invest Ophthalmol Vis Sci* **59**, 1360-1367
4. Pal, K., Mukadam, N., Petersen, I., and Cooper, C. (2018) Mild cognitive impairment and progression to dementia in people with diabetes, prediabetes and metabolic syndrome: a systematic review and meta-analysis. *Soc Psychiatry Psychiatr Epidemiol* **53**, 1149-1160
5. Ricci, G., Pirillo, I., Tomassoni, D., Sirignano, A., and Grappasonni, I. (2017) Metabolic syndrome, hypertension, and nervous system injury: Epidemiological correlates. *Clin Exp Hypertens* **39**, 8-16
6. Andica, C., Kamagata, K., Uchida, W., Takabayashi, K., Shimoji, K., Kaga, H., Someya, Y., Tamura, Y., Kawamori, R., Watada, H., Hori, M., and Aoki, S. (2022) White matter fiber-specific degeneration in older adults with metabolic syndrome. *Mol Metab* **62**, 101527
7. Andersen, C. J., Murphy, K. E., and Fernandez, M. L. (2016) Impact of Obesity and Metabolic Syndrome on Immunity. *Adv Nutr* **7**, 66-75

8. Berbudi, A., Rahmadika, N., Tjahjadi, A. I., and Ruslami, R. (2020) Type 2 Diabetes and its Impact on the Immune System. *Curr Diabetes Rev* **16**, 442-449
9. Jansen, I. E., Savage, J. E., Watanabe, K., Bryois, J., Williams, D. M., Steinberg, S., Sealock, J., Karlsson, I. K., Hagg, S., Athanasiu, L., Voyle, N., Proitsi, P., Witoelar, A., Stringer, S., Aarsland, D., Almdahl, I. S., Andersen, F., Bergh, S., Bettella, F., Bjornsson, S., Braekhus, A., Brathen, G., de Leeuw, C., Desikan, R. S., Djurovic, S., Dumitrescu, L., Fladby, T., Hohman, T. J., Jonsson, P. V., Kiddle, S. J., Rongve, A., Saltvedt, I., Sando, S. B., Selbaek, G., Shoai, M., Skene, N. G., Snaedal, J., Stordal, E., Ulstein, I. D., Wang, Y., White, L. R., Hardy, J., Hjerling-Leffler, J., Sullivan, P. F., van der Flier, W. M., Dobson, R., Davis, L. K., Stefansson, H., Stefansson, K., Pedersen, N. L., Ripke, S., Andreassen, O. A., and Posthuma, D. (2019) Genome-wide meta-analysis identifies new loci and functional pathways influencing Alzheimer's disease risk. *Nat Genet* **51**, 404-413
10. Johnson, E. C. B., Dammer, E. B., Duong, D. M., Ping, L., Zhou, M., Yin, L., Higginbotham, L. A., Guajardo, A., White, B., Troncoso, J. C., Thambisetty, M., Montine, T. J., Lee, E. B., Trojanowski, J. Q., Beach, T. G., Reiman, E. M., Haroutunian, V., Wang, M., Schadt, E., Zhang, B., Dickson, D. W., Ertekin-Taner, N., Golde, T. E., Petyuk, V. A., De Jager, P. L., Bennett, D. A., Wingo, T. S., Rangaraju, S., Hajjar, I., Shulman, J. M., Lah, J. J., Levey, A. I., and Seyfried, N. T. (2020) Large-scale proteomic analysis of Alzheimer's disease brain and cerebrospinal fluid reveals early changes in energy metabolism associated with microglia and astrocyte activation. *Nat Med* **26**, 769-780
11. Keren-Shaul, H., Spinrad, A., Weiner, A., Matcovitch-Natan, O., Dvir-Szternfeld, R., Ulland, T. K., David, E., Baruch, K., Lara-Astaiso, D., Toth, B., Itzkovitz, S., Colonna, M., Schwartz, M., and Amit, I. (2017) A Unique Microglia Type Associated with Restricting Development of Alzheimer's Disease. *Cell* **169**, 1276-1290 e1217
12. Krasemann, S., Madore, C., Cialic, R., Baufeld, C., Calcagno, N., El Fatimy, R., Beckers, L., O'Loughlin, E., Xu, Y., Fanek, Z., Greco, D. J., Smith, S. T., Tweet, G., Humulock, Z., Zrzavy, T., Conde-Sanroman, P., Gacias, M., Weng, Z., Chen, H., Tjon, E., Mazaheri, F., Hartmann, K., Madi, A., Ulrich, J. D., Glatzel, M., Worthmann, A., Heeren, J., Budnik, B., Lemere, C., Ikezu, T., Heppner, F. L., Litvak, V., Holtzman, D. M., Lassmann, H., Weiner, H. L., Ochando, J., Haass, C., and Butovsky, O. (2017) The TREM2-APOE Pathway Drives the Transcriptional Phenotype of Dysfunctional Microglia in Neurodegenerative Diseases. *Immunity* **47**, 566-581 e569
13. McQuade, A., and Blurton-Jones, M. (2019) Microglia in Alzheimer's Disease: Exploring How Genetics and Phenotype Influence Risk. *J Mol Biol* **431**, 1805-1817
14. Spangenberg, E., Severson, P. L., Hohsfield, L. A., Crapser, J., Zhang, J., Burton, E. A., Zhang, Y., Spevak, W., Lin, J., Phan, N. Y., Habets, G., Rymar, A., Tsang, G., Walters, J., Nespi, M., Singh, P., Broome, S., Ibrahim, P., Zhang, C., Bollag, G., West, B. L., and Green, K. N. (2019) Sustained microglial depletion with CSF1R inhibitor impairs parenchymal plaque development in an Alzheimer's disease model. *Nat Commun* **10**, 3758
15. Zhou, Y., Song, W. M., Andhey, P. S., Swain, A., Levy, T., Miller, K. R., Poliani, P. L., Cominelli, M., Grover, S., Gilfillan, S., Cella, M., Ulland, T. K., Zaitsev, K., Miyashita, A., Ikeuchi, T., Sainouchi, M., Kakita, A., Bennett, D. A., Schneider, J. A., Nichols, M. R., Beausoleil, S. A., Ulrich, J. D., Holtzman, D. M., Artyomov, M. N., and Colonna, M. (2020)

Human and mouse single-nucleus transcriptomics reveal TREM2-dependent and TREM2-independent cellular responses in Alzheimer's disease. *Nat Med* **26**, 131-142

16. Bisht, K., Okojie, K. A., Sharma, K., Lentferink, D. H., Sun, Y. Y., Chen, H. R., Uweru, J. O., Amancherla, S., Calcuttawala, Z., Campos-Salazar, A. B., Corliss, B., Jabbour, L., Benderoth, J., Friestad, B., Mills, W. A., 3rd, Isakson, B. E., Tremblay, M. E., Kuan, C. Y., and Eyo, U. B. (2021) Capillary-associated microglia regulate vascular structure and function through PANX1-P2RY12 coupling in mice. *Nat Commun* **12**, 5289
17. Butovsky, O., and Weiner, H. L. (2018) Microglial signatures and their role in health and disease. *Nat Rev Neurosci* **19**, 622-635
18. Csaszar, E., Lenart, N., Cserep, C., Kornyei, Z., Fekete, R., Posfai, B., Balazsfi, D., Hangya, B., Schwarcz, A. D., Szabadits, E., Szollosi, D., Szigeti, K., Mathe, D., West, B. L., Sviatko, K., Bras, A. R., Mariani, J. C., Kliewer, A., Lenkei, Z., Hricisak, L., Benyo, Z., Baranyi, M., Sperlagh, B., Menyhart, A., Farkas, E., and Denes, A. (2022) Microglia modulate blood flow, neurovascular coupling, and hypoperfusion via purinergic actions. *J Exp Med* **219**
19. Halder, S. K., and Milner, R. (2019) A critical role for microglia in maintaining vascular integrity in the hypoxic spinal cord. *Proc Natl Acad Sci U S A* **116**, 26029-26037
20. Mills, S. A., Jobling, A. I., Dixon, M. A., Bui, B. V., Vessey, K. A., Phipps, J. A., Greferath, U., Venables, G., Wong, V. H. Y., Wong, C. H. Y., He, Z., Hui, F., Young, J. C., Tonc, J., Ivanova, E., Sagdullaev, B. T., and Fletcher, E. L. (2021) Fractalkine-induced microglial vasoregulation occurs within the retina and is altered early in diabetic retinopathy. *Proc Natl Acad Sci U S A* **118**
21. Mondo, E., Becker, S. C., Kautzman, A. G., Schifferer, M., Baer, C. E., Chen, J., Huang, E. J., Simons, M., and Schafer, D. P. (2020) A Developmental Analysis of Juxtavascular Microglia Dynamics and Interactions with the Vasculature. *J Neurosci* **40**, 6503-6521
22. Hammond, T. R., Dufort, C., Dissing-Olesen, L., Giera, S., Young, A., Wysoker, A., Walker, A. J., Gergits, F., Segel, M., Nemesh, J., Marsh, S. E., Saunders, A., Macosko, E., Ginhoux, F., Chen, J., Franklin, R. J. M., Piao, X., McCarroll, S. A., and Stevens, B. (2019) Single-Cell RNA Sequencing of Microglia throughout the Mouse Lifespan and in the Injured Brain Reveals Complex Cell-State Changes. *Immunity* **50**, 253-271 e256
23. Sala Frigerio, C., Wolfs, L., Fattorelli, N., Thrupp, N., Voytyuk, I., Schmidt, I., Mancuso, R., Chen, W. T., Woodbury, M. E., Srivastava, G., Moller, T., Hudry, E., Das, S., Saido, T., Karran, E., Hyman, B., Perry, V. H., Fiers, M., and De Strooper, B. (2019) The Major Risk Factors for Alzheimer's Disease: Age, Sex, and Genes Modulate the Microglia Response to Abeta Plaques. *Cell Rep* **27**, 1293-1306 e1296
24. Yang, H. S., Onos, K. D., Choi, K., Keezer, K. J., Skelly, D. A., Carter, G. W., and Howell, G. R. (2021) Natural genetic variation determines microglia heterogeneity in wild-derived mouse models of Alzheimer's disease. *Cell Rep* **34**, 108739
25. Olah, M., Menon, V., Habib, N., Taga, M. F., Ma, Y., Yung, C. J., Cimpean, M., Khairallah, A., Coronas-Samano, G., Sankowski, R., Grun, D., Kroshilina, A. A., Dionne, D., Sarkis, R. A., Cosgrove, G. R., Helgager, J., Golden, J. A., Pennell, P. B., Prinz, M., Vonsattel, J. P. G., Teich, A. F., Schneider, J. A., Bennett, D. A., Regev, A., Elyaman, W., Bradshaw, E. M., and De Jager, P. L. (2020) Single cell RNA sequencing of human microglia uncovers a subset associated with Alzheimer's disease. *Nat Commun* **11**, 6129

26. Champy, M. F., Selloum, M., Zeitler, V., Caradec, C., Jung, B., Rousseau, S., Pouilly, L., Sorg, T., and Auwerx, J. (2008) Genetic background determines metabolic phenotypes in the mouse. *Mamm Genome* **19**, 318-331
27. Kluge, R., Scherneck, S., Schurmann, A., and Joost, H. G. (2012) Pathophysiology and genetics of obesity and diabetes in the New Zealand obese mouse: a model of the human metabolic syndrome. *Methods Mol Biol* **933**, 59-73
28. Lubura, M., Hesse, D., Kraemer, M., Hallahan, N., Schupp, M., von Loffelholz, C., Kriebel, J., Rudovich, N., Pfeiffer, A., John, C., Scheja, L., Heeren, J., Koliaki, C., Roden, M., and Schurmann, A. (2015) Diabetes prevalence in NZO females depends on estrogen action on liver fat content. *Am J Physiol Endocrinol Metab* **309**, E968-980
29. Marsh, S. E., Walker, A. J., Kamath, T., Dissing-Olesen, L., Hammond, T. R., de Soysa, T. Y., Young, A. M. H., Murphy, S., Abdulraouf, A., Nadaf, N., Dufort, C., Walker, A. C., Lucca, L. E., Kozareva, V., Vanderburg, C., Hong, S., Bulstrode, H., Hutchinson, P. J., Gaffney, D. J., Hafler, D. A., Franklin, R. J. M., Macosko, E. Z., and Stevens, B. (2022) Dissection of artifactual and confounding glial signatures by single-cell sequencing of mouse and human brain. *Nat Neurosci* **25**, 306-316
30. Heng, T. S., Painter, M. W., and Immunological Genome Project, C. (2008) The Immunological Genome Project: networks of gene expression in immune cells. *Nat Immunol* **9**, 1091-1094
31. Aran, D., Looney, A. P., Liu, L., Wu, E., Fong, V., Hsu, A., Chak, S., Naikawadi, R. P., Wolters, P. J., Abate, A. R., Butte, A. J., and Bhattacharya, M. (2019) Reference-based analysis of lung single-cell sequencing reveals a transitional profibrotic macrophage. *Nat Immunol* **20**, 163-172
32. Robinson, M. D., McCarthy, D. J., and Smyth, G. K. (2010) edgeR: a Bioconductor package for differential expression analysis of digital gene expression data. *Bioinformatics* **26**, 139-140
33. Squair, J. W., Gautier, M., Kathe, C., Anderson, M. A., James, N. D., Hutson, T. H., Hudelle, R., Qaiser, T., Matson, K. J. E., Barraud, Q., Levine, A. J., La Manno, G., Skinnider, M. A., and Courtine, G. (2021) Confronting false discoveries in single-cell differential expression. *Nat Commun* **12**, 5692
34. Qian, T., Wang, K., Cui, J., He, Y., and Yang, Z. (2016) Angiopoietin-Like Protein 7 Promotes an Inflammatory Phenotype in RAW264.7 Macrophages Through the P38 MAPK Signaling Pathway. *Inflammation* **39**, 974-985
35. Davalos, D., Ryu, J. K., Merlini, M., Baeten, K. M., Le Moan, N., Petersen, M. A., Deerinck, T. J., Smirnoff, D. S., Bedard, C., Hakozaki, H., Gonias Murray, S., Ling, J. B., Lassmann, H., Degen, J. L., Ellisman, M. H., and Akassoglou, K. (2012) Fibrinogen-induced perivascular microglial clustering is required for the development of axonal damage in neuroinflammation. *Nat Commun* **3**, 1227
36. Mendiola, A. S., Yan, Z., Dixit, K., Johnson, J. R., Bouhaddou, M., Meyer-Franke, A., Shin, M. G., Yong, Y., Agrawal, A., MacDonald, E., Muthukumar, G., Pearce, C., Arun, N., Cabriga, B., Meza-Acevedo, R., Alzamora, M., Zamvil, S. S., Pico, A. R., Ryu, J. K., Krogan, N. J., and Akassoglou, K. (2023) Defining blood-induced microglia functions in neurodegeneration through multiomic profiling. *Nat Immunol* **24**, 1173-1187

37. Kloske, C. M., Barnum, C. J., Batista, A. F., Bradshaw, E. M., Brickman, A. M., Bu, G., Dennison, J., Gearon, M. D., Goate, A. M., Haass, C., Heneka, M. T., Hu, W. T., Huggins, L. K. L., Jones, N. S., Koldamova, R., Lemere, C. A., Liddelow, S. A., Marcora, E., Marsh, S. E., Nielsen, H. M., Petersen, K. K., Petersen, M., Pina-Escudero, S. D., Qiu, W. Q., Quiroz, Y. T., Reiman, E., Sexton, C., Tansey, M. G., Tcw, J., Teunissen, C. E., Tijms, B. M., van der Kant, R., Wallings, R., Weninger, S. C., Wharton, W., Wilcock, D. M., Wishard, T. J., Worley, S. L., Zetterberg, H., and Carrillo, M. C. (2023) APOE and immunity: Research highlights. *Alzheimers Dement* **19**, 2677-2696

38. Hultman, K., Strickland, S., and Norris, E. H. (2013) The APOE varepsilon4/varepsilon4 genotype potentiates vascular fibrin(ogen) deposition in amyloid-laden vessels in the brains of Alzheimer's disease patients. *J Cereb Blood Flow Metab* **33**, 1251-1258

39. Kucukdereli, H., Allen, N. J., Lee, A. T., Feng, A., Ozlu, M. I., Conatser, L. M., Chakraborty, C., Workman, G., Weaver, M., Sage, E. H., Barres, B. A., and Eroglu, C. (2011) Control of excitatory CNS synaptogenesis by astrocyte-secreted proteins Hevin and SPARC. *Proc Natl Acad Sci U S A* **108**, E440-449

40. Kierdorf, K., Erny, D., Goldmann, T., Sander, V., Schulz, C., Perdiguero, E. G., Wieghofer, P., Heinrich, A., Riemke, P., Holscher, C., Muller, D. N., Luckow, B., Brocker, T., Debowski, K., Fritz, G., Opdenakker, G., Diefenbach, A., Biber, K., Heikenwalder, M., Geissmann, F., Rosenbauer, F., and Prinz, M. (2013) Microglia emerge from erythromyeloid precursors via Pu.1- and Irf8-dependent pathways. *Nat Neurosci* **16**, 273-280

41. Liu, Z., Xu, J., Ma, Q., Zhang, X., Yang, Q., Wang, L., Cao, Y., Xu, Z., Tawfik, A., Sun, Y., Weintraub, N. L., Fulton, D. J., Hong, M., Dong, Z., Smith, L. E. H., Caldwell, R. B., Sodhi, A., and Huo, Y. (2020) Glycolysis links reciprocal activation of myeloid cells and endothelial cells in the retinal angiogenic niche. *Sci Transl Med* **12**

42. Soehnlein, O., Drechsler, M., Doring, Y., Lievens, D., Hartwig, H., Kemmerich, K., Ortega-Gomez, A., Mandl, M., Vijayan, S., Projahn, D., Garlichs, C. D., Koenen, R. R., Hristov, M., Lutgens, E., Zernecke, A., and Weber, C. (2013) Distinct functions of chemokine receptor axes in the atherogenic mobilization and recruitment of classical monocytes. *EMBO Mol Med* **5**, 471-481

43. Massberg, S., Enders, G., Matos, F. C., Tomic, L. I., Leiderer, R., Eisenmenger, S., Messmer, K., and Krombach, F. (1999) Fibrinogen deposition at the postischemic vessel wall promotes platelet adhesion during ischemia-reperfusion in vivo. *Blood* **94**, 3829-3838

44. Vilar, R., Fish, R. J., Casini, A., and Neerman-Arbez, M. (2020) Fibrin(ogen) in human disease: both friend and foe. *Haematologica* **105**, 284-296

45. Samadi, M., Moradi, S., Moradinazar, M., Mostafai, R., and Pasdar, Y. (2019) Dietary pattern in relation to the risk of Alzheimer's disease: a systematic review. *Neurol Sci* **40**, 2031-2043

46. Jankowsky, J. L., Fadale, D. J., Anderson, J., Xu, G. M., Gonzales, V., Jenkins, N. A., Copeland, N. G., Lee, M. K., Younkin, L. H., Wagner, S. L., Younkin, S. G., and Borchelt, D. R. (2004) Mutant presenilins specifically elevate the levels of the 42 residue beta-amyloid peptide in vivo: evidence for augmentation of a 42-specific gamma secretase. *Hum Mol Genet* **13**, 159-170

47. Kiani Shabestari, S., Morabito, S., Danhash, E. P., McQuade, A., Sanchez, J. R., Miyoshi, E., Chadarevian, J. P., Claes, C., Coburn, M. A., Hasselmann, J., Hidalgo, J., Tran, K. N.,

Martini, A. C., Chang Rothermich, W., Pascual, J., Head, E., Hume, D. A., Pridans, C., Davtyan, H., Swarup, V., and Blurton-Jones, M. (2022) Absence of microglia promotes diverse pathologies and early lethality in Alzheimer's disease mice. *Cell Rep* **39**, 110961

48. Chen, Y., and Colonna, M. (2021) Microglia in Alzheimer's disease at single-cell level. Are there common patterns in humans and mice? *J Exp Med* **218**
49. Huang, Y., and Mahley, R. W. (2014) Apolipoprotein E: structure and function in lipid metabolism, neurobiology, and Alzheimer's diseases. *Neurobiol Dis* **72 Pt A**, 3-12
50. Khalil, Y. A., Rabes, J. P., Boileau, C., and Varret, M. (2021) APOE gene variants in primary dyslipidemia. *Atherosclerosis* **328**, 11-22
51. Karakaslar, E. O., Katiyar, N., Hasham, M., Youn, A., Sharma, S., Chung, C. H., Marches, R., Korstanje, R., Banchereau, J., and Ucar, D. (2023) Transcriptional activation of Jun and Fos members of the AP-1 complex is a conserved signature of immune aging that contributes to inflammaging. *Aging Cell* **22**, e13792
52. Furuichi, K., Gao, J. L., Horuk, R., Wada, T., Kaneko, S., and Murphy, P. M. (2008) Chemokine receptor CCR1 regulates inflammatory cell infiltration after renal ischemia-reperfusion injury. *J Immunol* **181**, 8670-8676
53. Li, P., Wang, L., Zhou, Y., Gan, Y., Zhu, W., Xia, Y., Jiang, X., Watkins, S., Vazquez, A., Thomson, A. W., Chen, J., Yu, W., and Hu, X. (2017) C-C Chemokine Receptor Type 5 (CCR5)-Mediated Docking of Transferred Tregs Protects Against Early Blood-Brain Barrier Disruption After Stroke. *J Am Heart Assoc* **6**
54. Zhang, Z., Wang, Q., Yao, J., Zhou, X., Zhao, J., Zhang, X., Dong, J., and Liao, L. (2020) Chemokine Receptor 5, a Double-Edged Sword in Metabolic Syndrome and Cardiovascular Disease. *Front Pharmacol* **11**, 146
55. Marchesi, C., Ebrahimian, T., Angulo, O., Paradis, P., and Schiffrin, E. L. (2009) Endothelial nitric oxide synthase uncoupling and perivascular adipose oxidative stress and inflammation contribute to vascular dysfunction in a rodent model of metabolic syndrome. *Hypertension* **54**, 1384-1392
56. Siddiqui, M. R., Mayanil, C. S., Kim, K. S., and Tomita, T. (2015) Angiopoietin-1 Regulates Brain Endothelial Permeability through PTPN-2 Mediated Tyrosine Dephosphorylation of Occludin. *PLoS One* **10**, e0130857
57. Freeman, B. D., Machado, F. S., Tanowitz, H. B., and Desruisseaux, M. S. (2014) Endothelin-1 and its role in the pathogenesis of infectious diseases. *Life Sci* **118**, 110-119
58. Wang, M., Hao, H., Leeper, N. J., Zhu, L., and Early Career, C. (2018) Thrombotic Regulation From the Endothelial Cell Perspectives. *Arterioscler Thromb Vasc Biol* **38**, e90-e95
59. Li, X., Li, Y., Jin, Y., Zhang, Y., Wu, J., Xu, Z., Huang, Y., Cai, L., Gao, S., Liu, T., Zeng, F., Wang, Y., Wang, W., Yuan, T. F., Tian, H., Shu, Y., Guo, F., Lu, W., Mao, Y., Mei, X., Rao, Y., and Peng, B. (2023) Transcriptional and epigenetic decoding of the microglial aging process. *Nat Aging*
60. Hou, J., Chen, Y., Grajales-Reyes, G., and Colonna, M. (2022) TREM2 dependent and independent functions of microglia in Alzheimer's disease. *Mol Neurodegener* **17**, 84
61. Gomez, G., Beason-Held, L. L., Bilgel, M., An, Y., Wong, D. F., Studenski, S., Ferrucci, L., and Resnick, S. M. (2018) Metabolic Syndrome and Amyloid Accumulation in the Aging Brain. *J Alzheimers Dis* **65**, 629-639

62. Pillai, J. A., Bena, J., Bekris, L., Kodur, N., Kasumov, T., Leverenz, J. B., Kashyap, S. R., and Alzheimer's Disease Neuroimaging, I. (2023) Metabolic syndrome biomarkers relate to rate of cognitive decline in MCI and dementia stages of Alzheimer's disease. *Alzheimers Res Ther* **15**, 54
63. Verdile, G., Keane, K. N., Cruzat, V. F., Medic, S., Sabale, M., Rowles, J., Wijesekara, N., Martins, R. N., Fraser, P. E., and Newsholme, P. (2015) Inflammation and Oxidative Stress: The Molecular Connectivity between Insulin Resistance, Obesity, and Alzheimer's Disease. *Mediators Inflamm* **2015**, 105828
64. Lou, N., Takano, T., Pei, Y., Xavier, A. L., Goldman, S. A., and Nedergaard, M. (2016) Purinergic receptor P2RY12-dependent microglial closure of the injured blood-brain barrier. *Proc Natl Acad Sci U S A* **113**, 1074-1079
65. Niedowicz, D. M., Reeves, V. L., Platt, T. L., Kohler, K., Beckett, T. L., Powell, D. K., Lee, T. L., Sexton, T. R., Song, E. S., Brewer, L. D., Latimer, C. S., Kraner, S. D., Larson, K. L., Ozcan, S., Norris, C. M., Hersh, L. B., Porter, N. M., Wilcock, D. M., and Murphy, M. P. (2014) Obesity and diabetes cause cognitive dysfunction in the absence of accelerated beta-amyloid deposition in a novel murine model of mixed or vascular dementia. *Acta Neuropathol Commun* **2**, 64
66. Cheng, Z., Dai, L., Wu, Y., Cao, Y., Chai, X., Wang, P., Liu, C., Ni, M., Gao, F., Wang, Q., and Lv, X. (2023) Correlation of blood-brain barrier leakage with cerebral small vessel disease including cerebral microbleeds in Alzheimer's disease. *Front Neurol* **14**, 1077860
67. Cordonnier, C., and van der Flier, W. M. (2011) Brain microbleeds and Alzheimer's disease: innocent observation or key player? *Brain* **134**, 335-344
68. Dierksen, G. A., Skehan, M. E., Khan, M. A., Jeng, J., Nandigam, R. N., Becker, J. A., Kumar, A., Neal, K. L., Betensky, R. A., Frosch, M. P., Rosand, J., Johnson, K. A., Viswanathan, A., Salat, D. H., and Greenberg, S. M. (2010) Spatial relation between microbleeds and amyloid deposits in amyloid angiopathy. *Ann Neurol* **68**, 545-548
69. Cajamarca, S. A., Norris, E. H., van der Weerd, L., Strickland, S., and Ahn, H. J. (2020) Cerebral amyloid angiopathy-linked beta-amyloid mutations promote cerebral fibrin deposits via increased binding affinity for fibrinogen. *Proc Natl Acad Sci U S A* **117**, 14482-14492
70. Freeze, W. M., Bacskai, B. J., Frosch, M. P., Jacobs, H. I. L., Backes, W. H., Greenberg, S. M., and van Veluw, S. J. (2019) Blood-Brain Barrier Leakage and Microvascular Lesions in Cerebral Amyloid Angiopathy. *Stroke* **50**, 328-335
71. Paneni, F., Beckman, J. A., Creager, M. A., and Cosentino, F. (2013) Diabetes and vascular disease: pathophysiology, clinical consequences, and medical therapy: part I. *European Heart Journal* **34**, 2436-2443

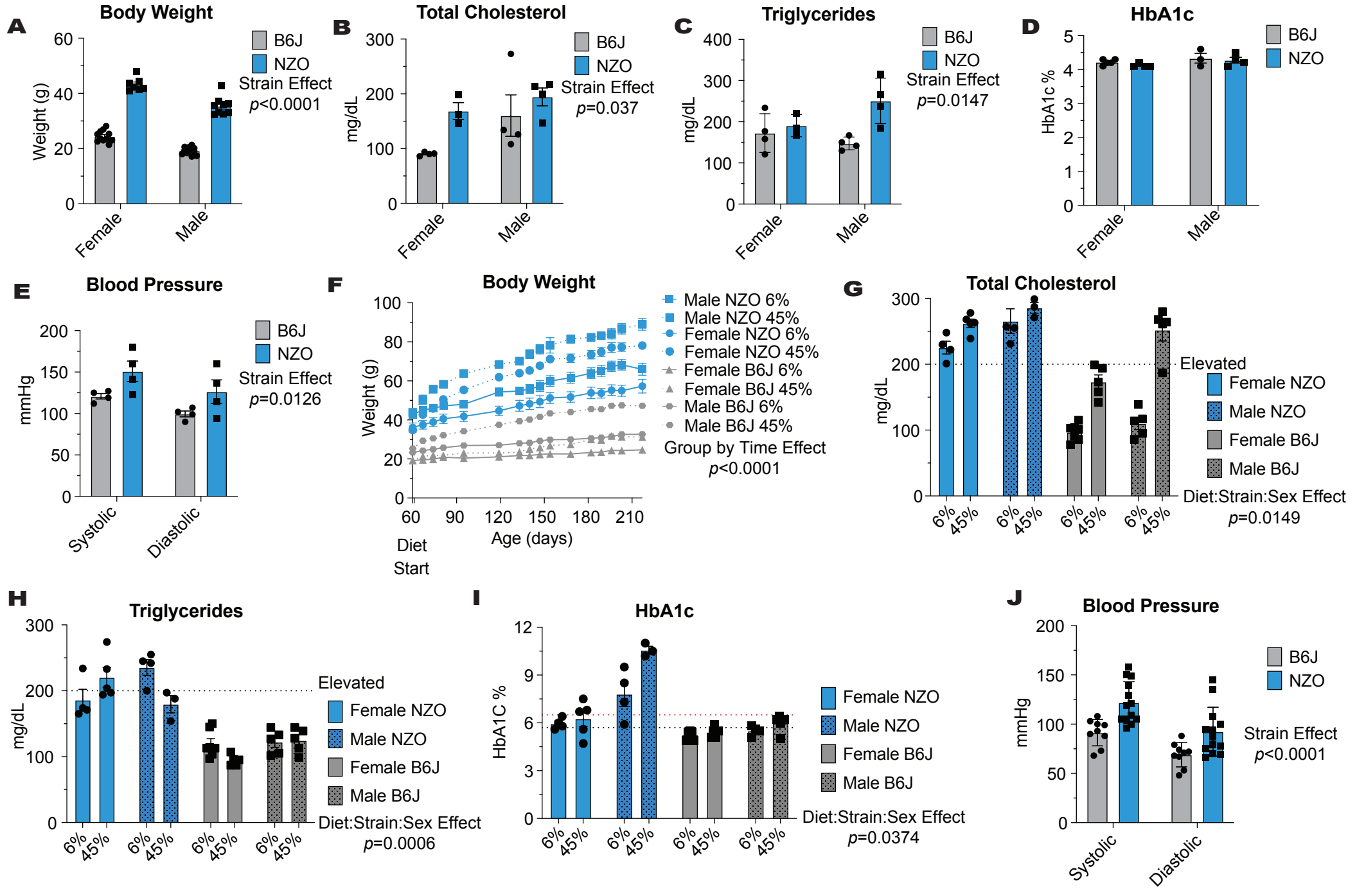
A
Body Weight
Weight (g)
B6J
NZO
Strain Effect
p<0.0001
Female
Male
B
Total Cholesterol
mg/dL
Strain Effect
p=0.037
C
Triglycerides
Strain Effect
p=0.0147
D
HbA1c
HbA1c %
E
Blood Pressure
mmHg
Strain Effect
p=0.0126
Systolic
Diastolic
F
Body Weight
Weight (g)
Male NZO 6%
Male NZO 45%
Female NZO 6%
Female NZO 45%
Female B6J 6%
Female B6J 45%
Male B6J 6%
Male B6J 45%
Group by Time Effect
p<0.0001
Diet Start
Age (days)
G
Total Cholesterol
mg/dL
Elevated
Female NZO
Male NZO
Female B6J
Male B6J
Diet:Strain:Sex Effect
p=0.0149
6%
45%
H
Triglycerides
mg/dL
Elevated
Female NZO
Male NZO
Female B6J
Male B6J
Diet:Strain:Sex Effect
p=0.0006
I
HbA1c
HbA1C %
Female NZO
Male NZO
Female B6J
Male B6J
Diet:Strain:Sex Effect
p=0.0374
J
Blood Pressure
mmHg
B6J
NZO
Strain Effect
p<0.0001
Systolic
Diastolic

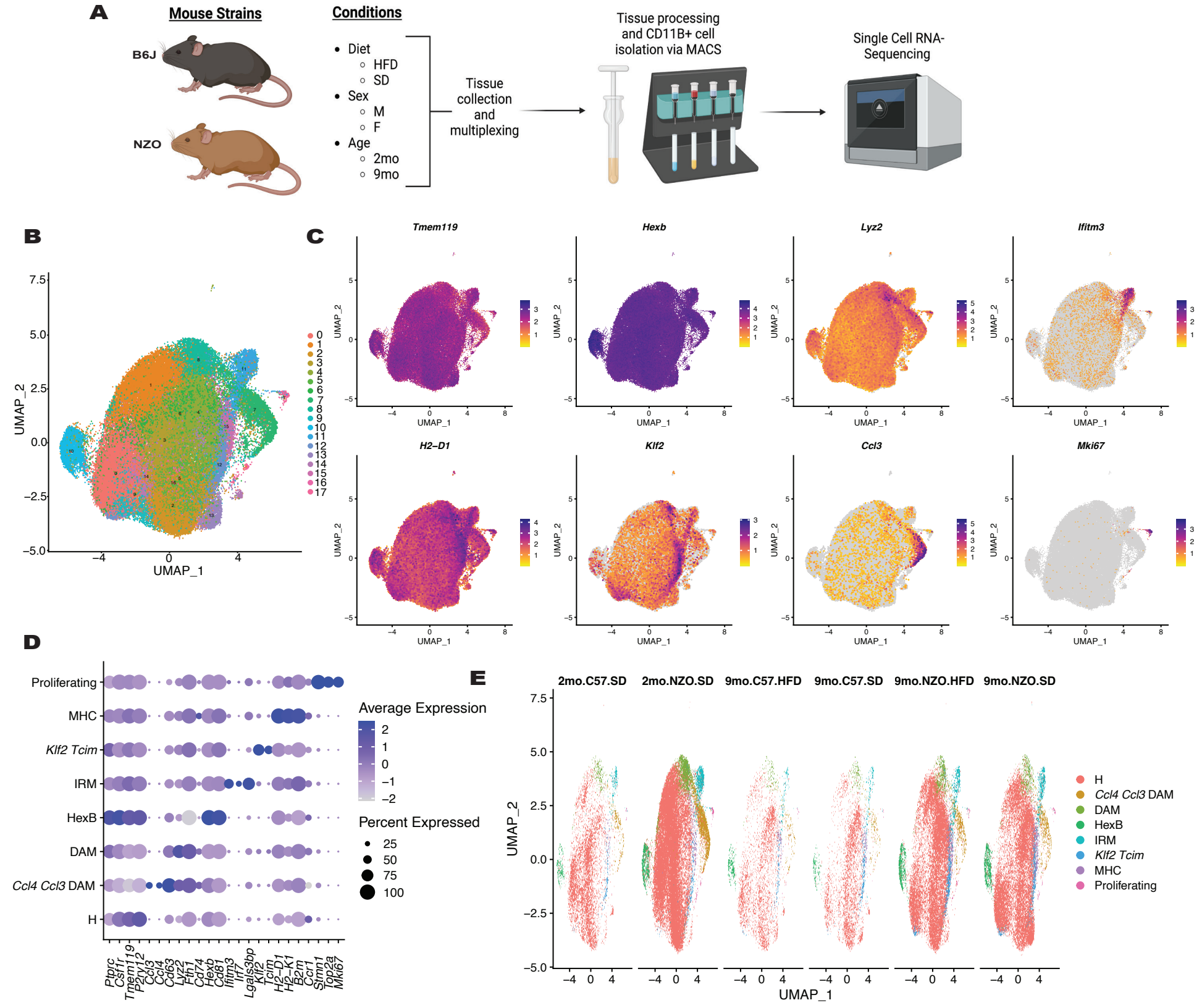
A
Mouse Strains
B6J
NZO
Conditions
Diet
HFD
SD
Sex
M
F
Age
2mo
9mo
Tissue collection and multiplexing
Tissue processing and CD11B+ cell isolation via MACS
Single Cell RNA-Sequencing
B
UMAP_1
UMAP_2
C
Tmem119
Hexb
Lyz2
Ifitm3
H2–D1
Klf2
Ccl3
Mki67
D
Proliferating
MHC
Klf2 Tcim
IRM
HexB
DAM
Ccl4 Ccl3 DAM
H
Ptprc
Csf1r
Tmem119
P2ry12
Ccl3
Ccl4
Cd63
Lyz2
Fth1
Cd74
Hexb
Cd81
Ifitm3
Irf7
Lgals3bp
Klf2
Tcim
H2–D1
H2–K1
B2m
Ccr1
Stmn1
Top2a
Mki67
Average Expression
Percent Expressed
25
50
75
100
E
2mo.C57.SD
2mo.NZO.SD
9mo.C57.HFD
9mo.C57.SD
9mo.NZO.HFD
9mo.NZO.SD
H
Ccl4 Ccl3 DAM
DAM
HexB
IRM
Klf2 Tcim
MHC
Proliferating

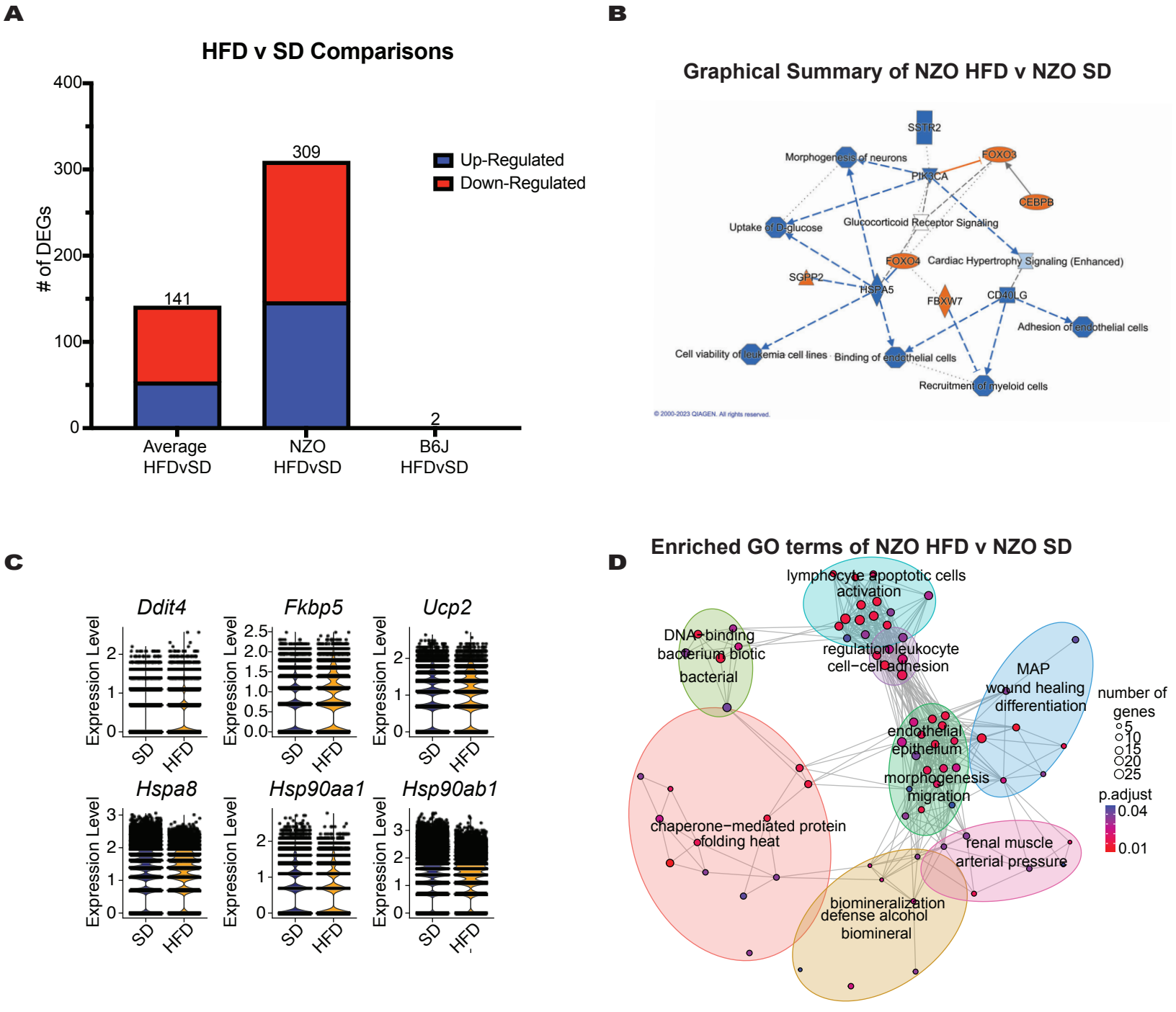
A
HFD v SD Comparisons
# of DEGs
400
300
200
100
0
141
309
2
Up-Regulated
Down-Regulated
Average HFDvSD
NZO HFDvSD
B6J HFDvSD
B
Graphical Summary of NZO HFD v NZO SD
SSTR2
Morphogenesis of neurons
FOXO3
PIK3CA
CEBPB
Uptake of D-glucose
Glucocorticoid Receptor Signaling
FOXO4
Cardiac Hypertrophy Signaling (Enhanced)
SGPP2
HSPA5
FBXW7
CD40LG
Adhesion of endothelial cells
Cell viability of leukemia cell lines
Binding of endothelial cells
Recruitment of myeloid cells
© 2000-2023 QIAGEN. All rights reserved.
C
Ddit4
Fkbp5
Ucp2
Hspa8
Hsp90aa1
Hsp90ab1
Expression Level
SD
HFD
D
Enriched GO terms of NZO HFD v NZO SD
lymphocyte apoptotic cells activation
DNA-binding bacterium biotic bacterial
regulation leukocyte cell−cell adhesion
MAP wound healing differentiation
endothelial epithelium morphogenesis migration
chaperone−mediated protein folding heat
renal muscle arterial pressure
biomineralization defense alcohol biomineral
number of genes
5
10
15
20
25
p.adjust
0.04
0.01

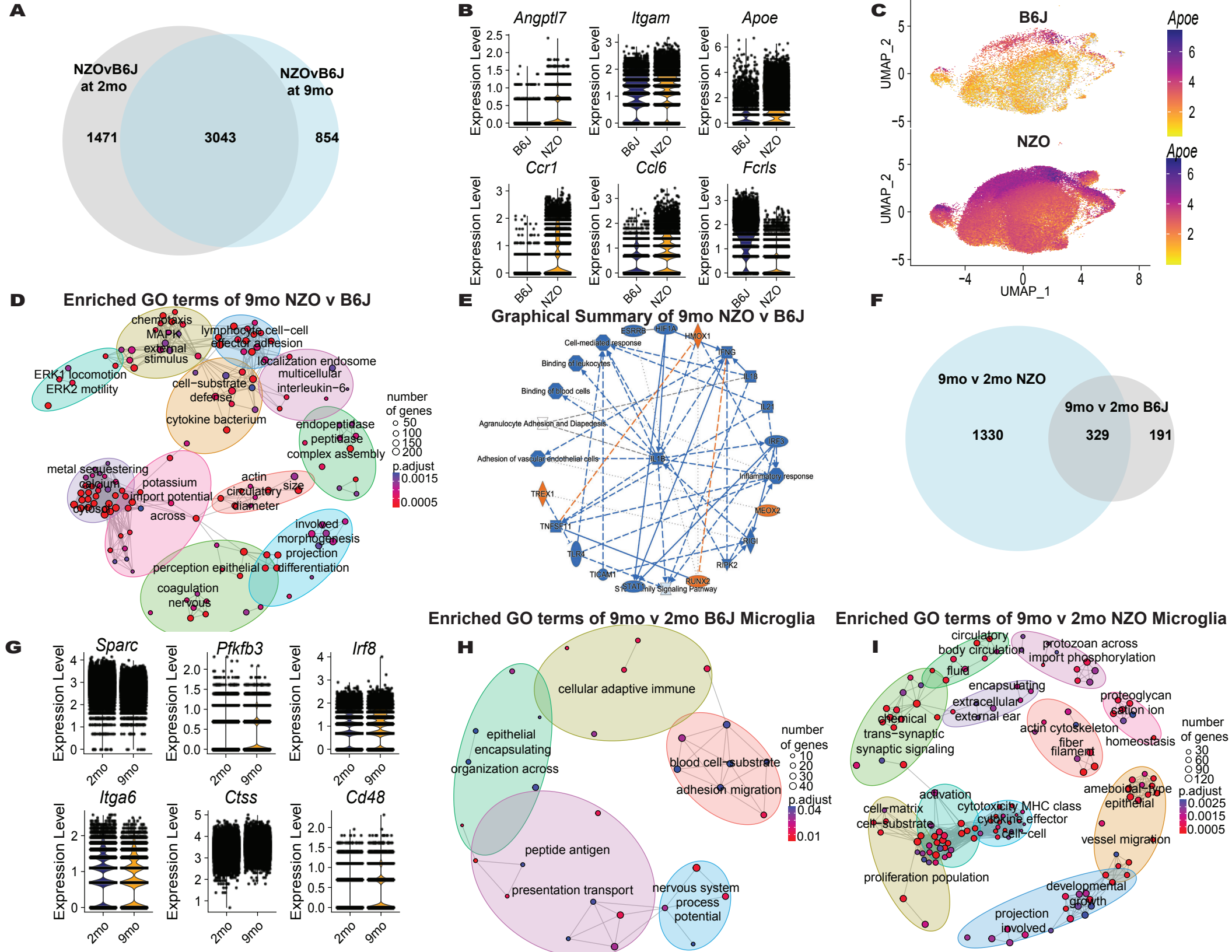
A
NZOvB6J at 2mo
NZOvB6J at 9mo
1471
3043
854
B
Angptl7
Itgam
Apoe
Ccr1
Ccl6
Fcrls
Expression Level
B6J
NZO
C
B6J
NZO
Apoe
UMAP_1
UMAP_2
D
Enriched GO terms of 9mo NZO v B6J
chemotaxis
MAPK external stimulus
lymphocyte cell−cell effector adhesion
localization endosome multicellular
interleukin−6
ERK1 locomotion
ERK2 motility
cell−substrate defense
cytokine bacterium
endopeptidase peptidase complex assembly
metal sequestering
calcium
potassium import potential
cytosol
across
actin circulatory size diameter
involved morphogenesis projection differentiation
perception epithelial
coagulation nervous
number of genes
50
100
150
200
p.adjust
0.0015
0.0005
E
Graphical Summary of 9mo NZO v B6J
ESRRB
HIF1A
HMOX1
Cell-mediated response
IFNG
Binding of leukocytes
IL18
Binding of blood cells
IL21
Agranulocyte Adhesion and Diapedesis
IRF3
Adhesion of vascular endothelial cells
IL1B
Inflammatory response
TREX1
MEOX2
TNFSF11
RIGI
TLR4
RIPK2
TICAM1
RUNX2
STAT1
Signaling Pathway
F
9mo v 2mo NZO
9mo v 2mo B6J
1330
329
191
G
Sparc
Pfkfb3
Irf8
Itga6
Ctss
Cd48
Expression Level
2mo
9mo
H
Enriched GO terms of 9mo v 2mo B6J Microglia
cellular adaptive immune
epithelial encapsulating organization across
blood cell−substrate adhesion migration
peptide antigen
presentation transport
nervous system process potential
number of genes
10
20
30
40
p.adjust
0.04
0.01
I
Enriched GO terms of 9mo v 2mo NZO Microglia
circulatory body circulation fluid
protozoan across import phosphorylation
encapsulating extracellular external ear
proteoglycan cation ion
chemical trans−synaptic synaptic signaling
actin cytoskeleton fiber filament
homeostasis
activation
cytotoxicity MHC class cytokine effector cell−cell
cell−matrix cell−substrate
ameboidal type epithelial
vessel migration
proliferation population
developmental growth
projection involved
number of genes
30
60
90
120
p.adjust
0.0025
0.0015
0.0005

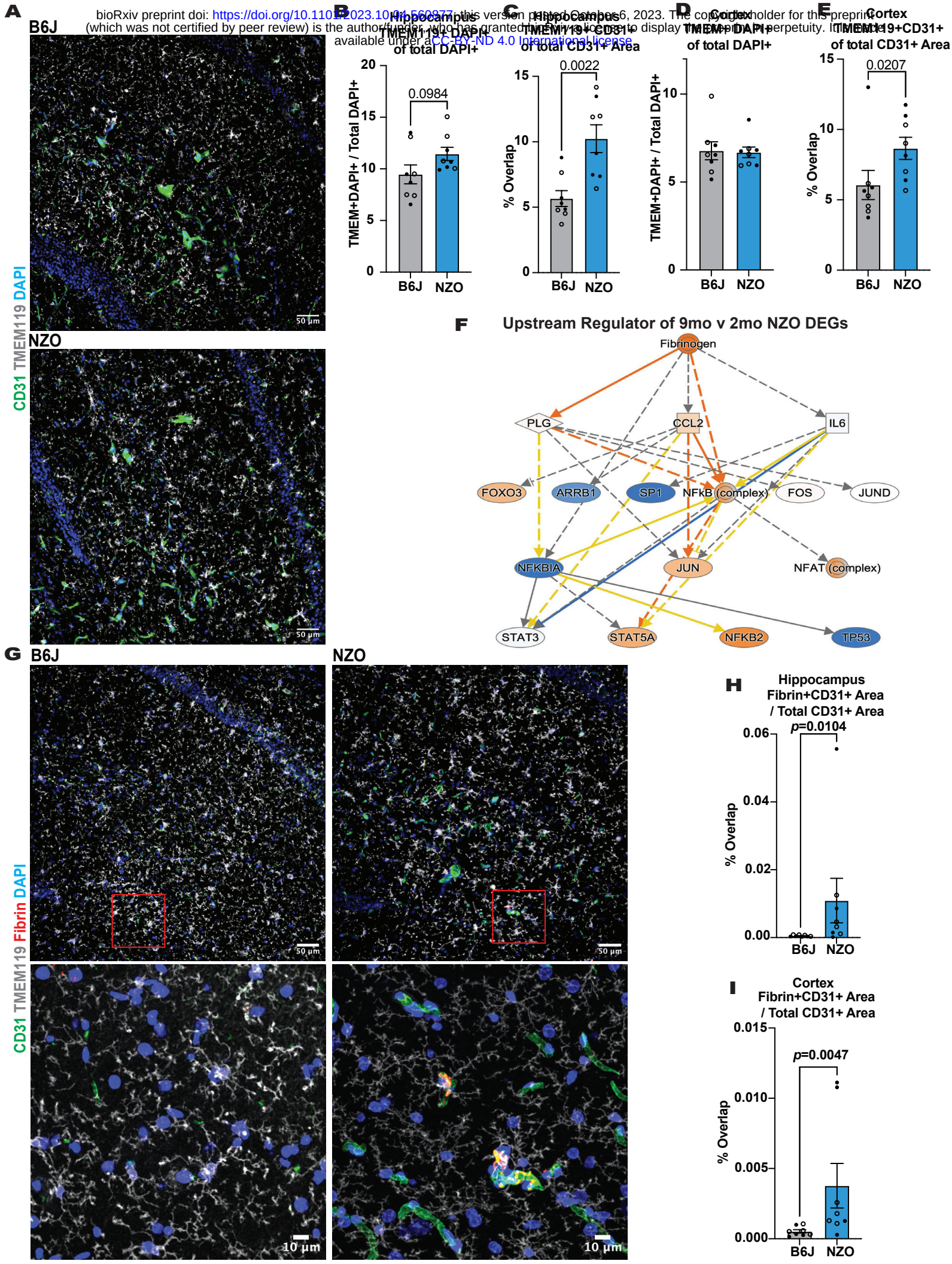

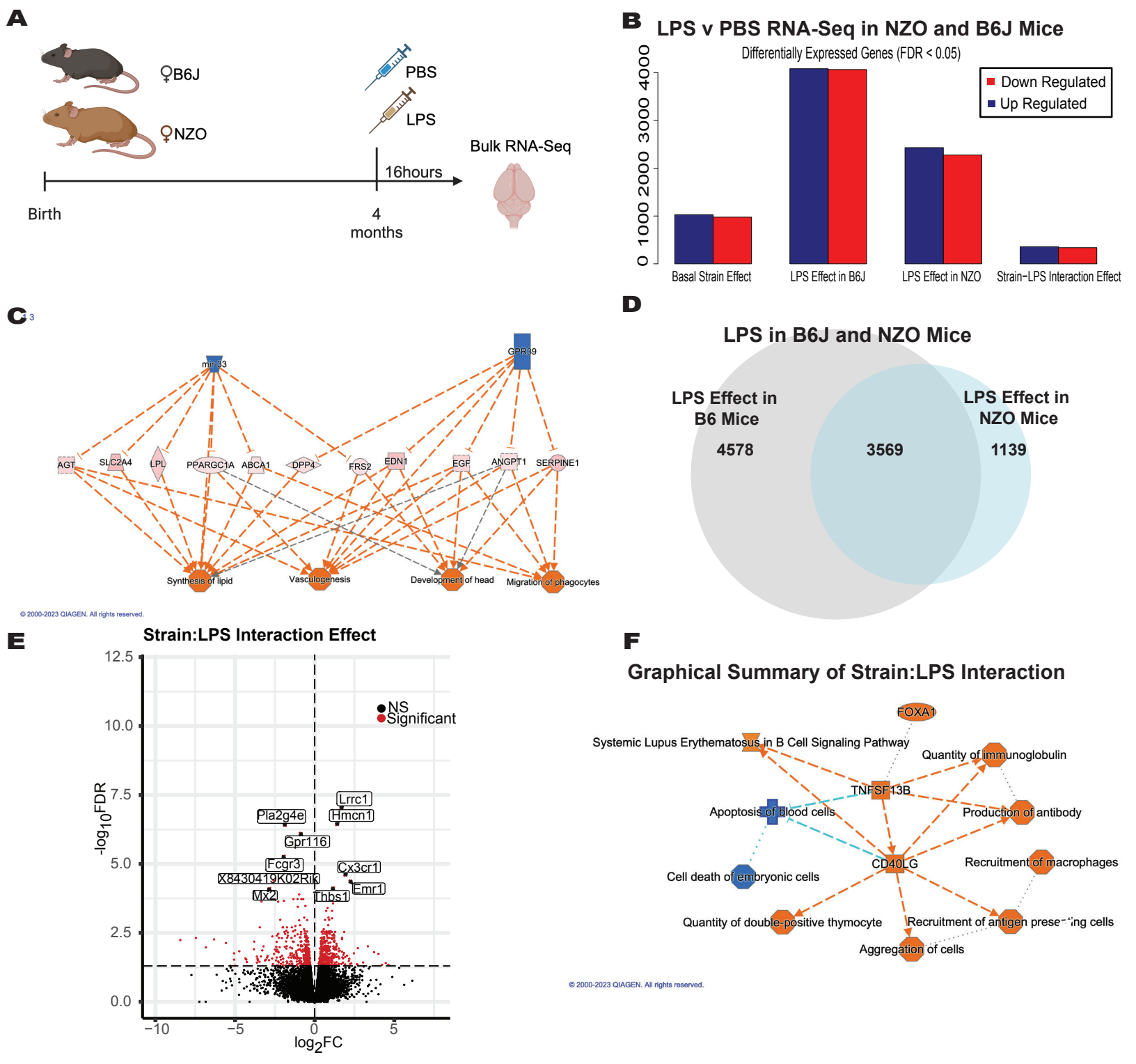
A
♀B6J
♀NZO
PBS
LPS
16hours
Bulk RNA-Seq
Birth
4
months
B
LPS v PBS RNA-Seq in NZO and B6J Mice
Differentially Expressed Genes (FDR < 0.05)
Down Regulated
Up Regulated
0 1000 2000 3000 4000
Basal Strain Effect
LPS Effect in B6J
LPS Effect in NZO
Strain−LPS Interaction Effect
C
miR-33
GPR39
AGT
SLC2A4
LPL
PPARGC1A
ABCA1
DPP4
FRS2
EDN1
EGF
ANGPT1
SERPINE1
Synthesis of lipid
Vasculogenesis
Development of head
Migration of phagocytes
© 2000-2023 QIAGEN. All rights reserved.
D
LPS in B6J and NZO Mice
LPS Effect in B6 Mice
4578
3569
LPS Effect in NZO Mice
1139
E
Strain:LPS Interaction Effect
NS
Significant
-log10FDR
log2FC
12.5
10.0
7.5
5.0
2.5
0.0
−10
−5
0
5
Lrrc1
Hmcn1
Pla2g4e
Gpr116
Fcgr3
Cx3cr1
X8430419K02Rik
Emr1
Mx2
Thbs1
F
Graphical Summary of Strain:LPS Interaction
FOXA1
Systemic Lupus Erythematosus in B Cell Signaling Pathway
Quantity of immunoglobulin
TNFSF13B
Apoptosis of blood cells
Production of antibody
CD40LG
Recruitment of macrophages
Cell death of embryonic cells
Quantity of double-positive thymocyte
Recruitment of antigen presenting cells
Aggregation of cells
© 2000-2023 QIAGEN. All rights reserved.

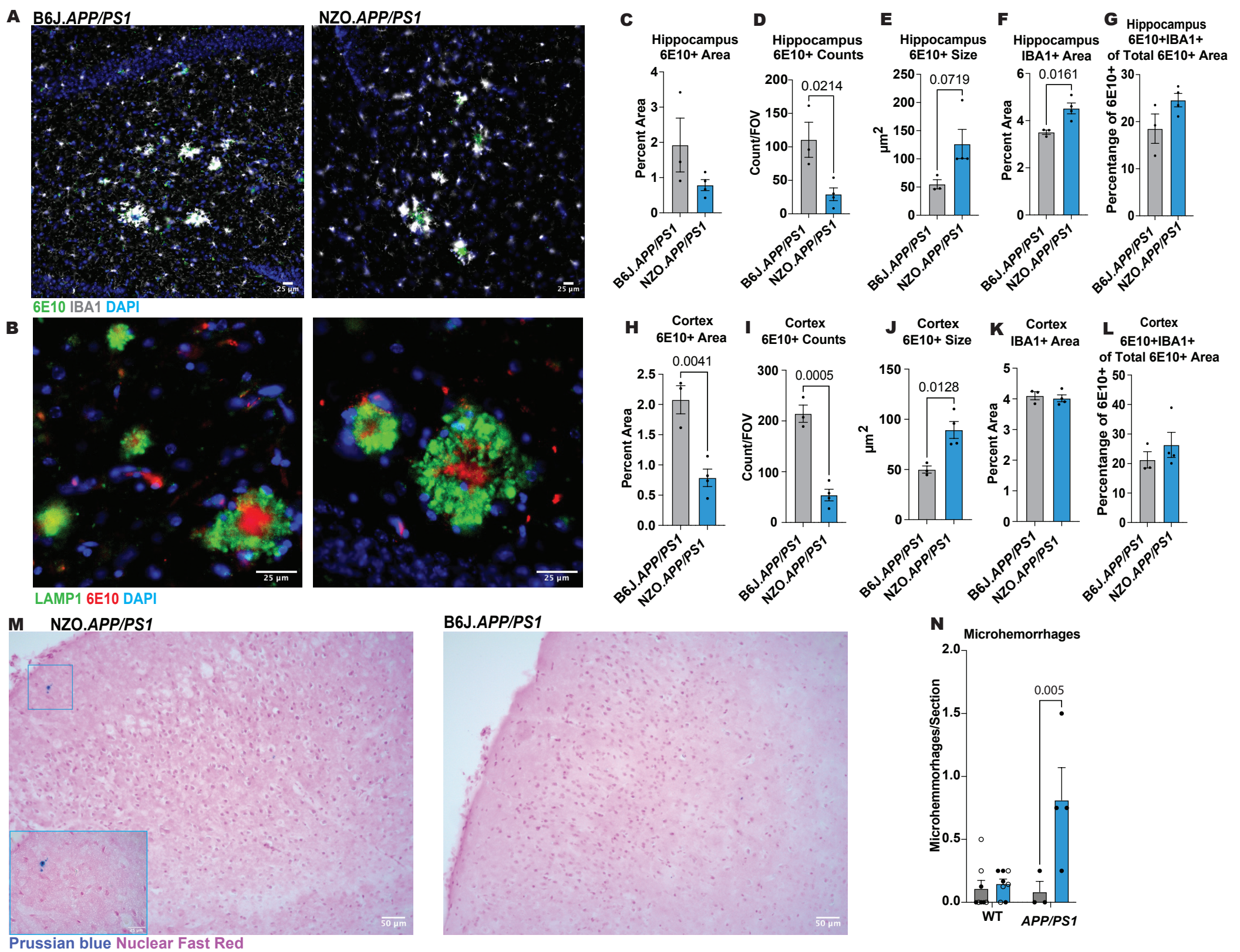
A
B6J.APP/PS1
NZO.APP/PS1
25 µm
6E10 IBA1 DAPI
B
LAMP1 6E10 DAPI
C
Hippocampus 6E10+ Area
Percent Area
D
Hippocampus 6E10+ Counts
Count/FOV
0.0214
E
Hippocampus 6E10+ Size
µm2
0.0719
F
Hippocampus IBA1+ Area
Percent Area
0.0161
G
Hippocampus 6E10+IBA1+ of Total 6E10+ Area
Percentage of 6E10+
H
Cortex 6E10+ Area
0.0041
I
Cortex 6E10+ Counts
0.0005
J
Cortex 6E10+ Size
0.0128
K
Cortex IBA1+ Area
L
Cortex 6E10+IBA1+ of Total 6E10+ Area
B6J.APP/PS1
NZO.APP/PS1
M
NZO.APP/PS1
B6J.APP/PS1
50 µm
Prussian blue Nuclear Fast Red
N
Microhemorrhages
Microhemmorhages/Section
0.005
WT
APP/PS1

A.

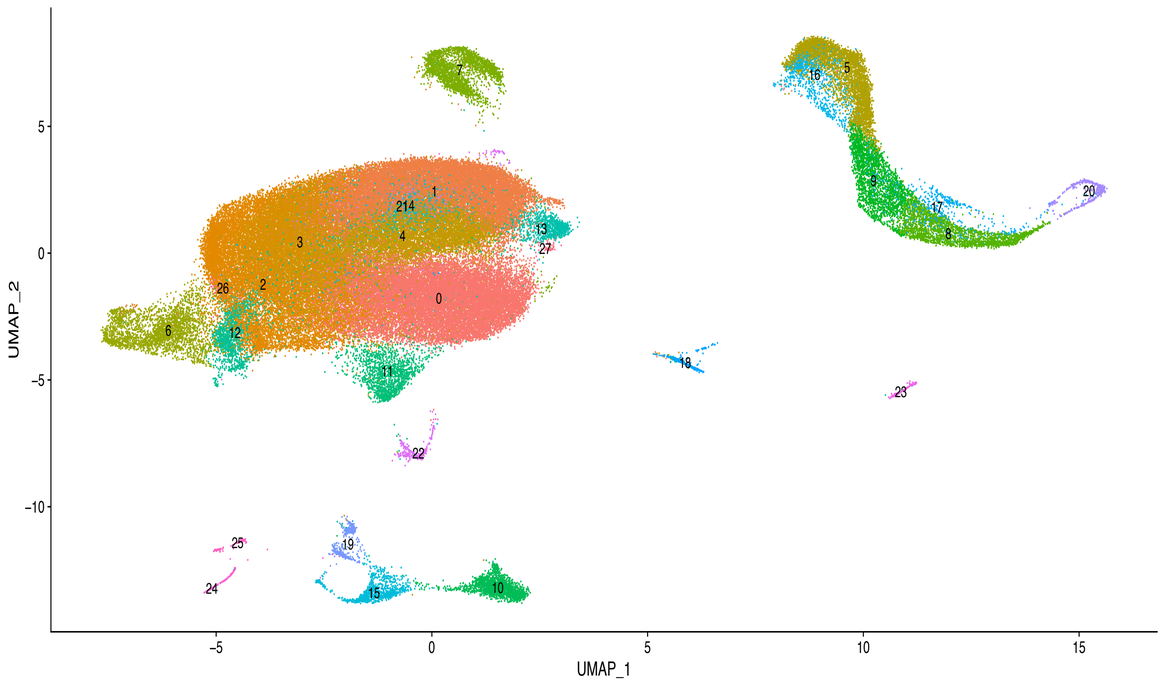

B.

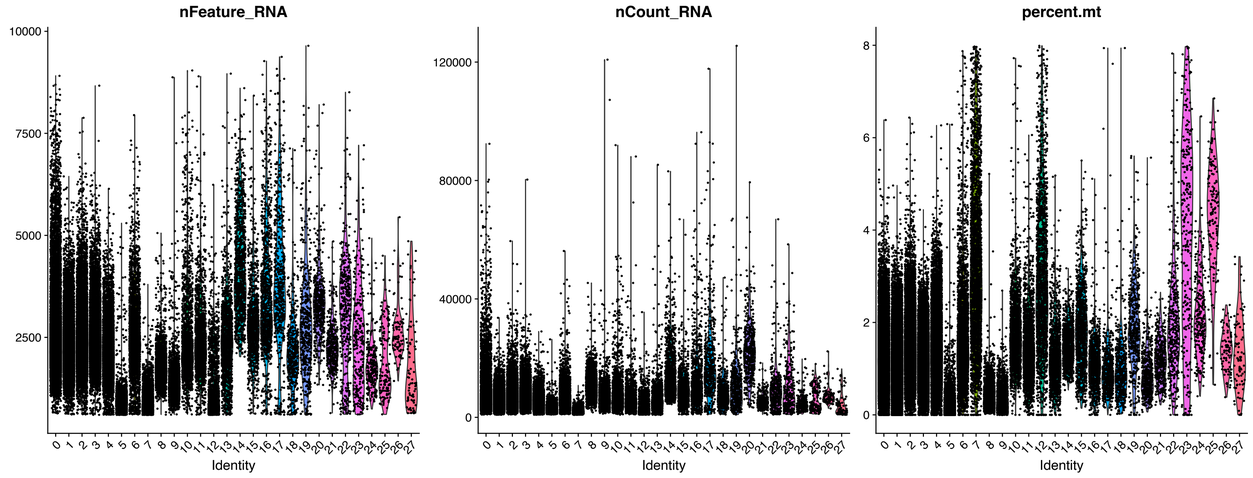

C.

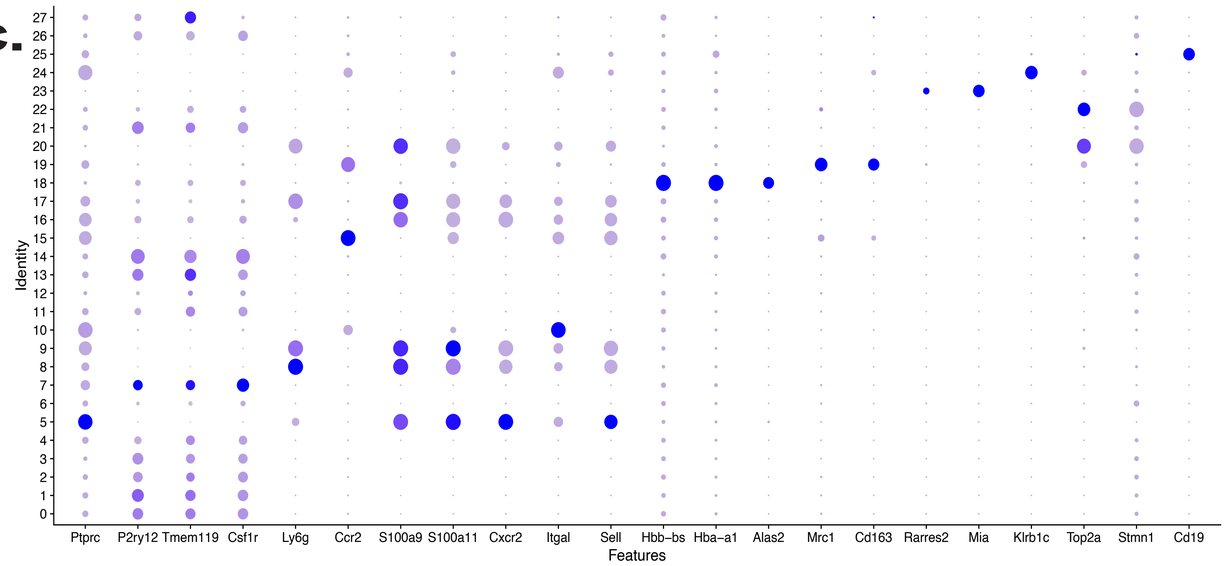

D.

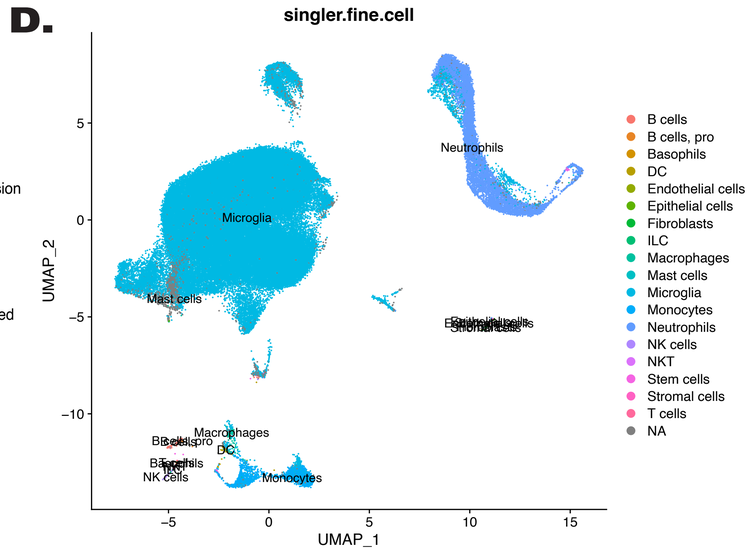

E.

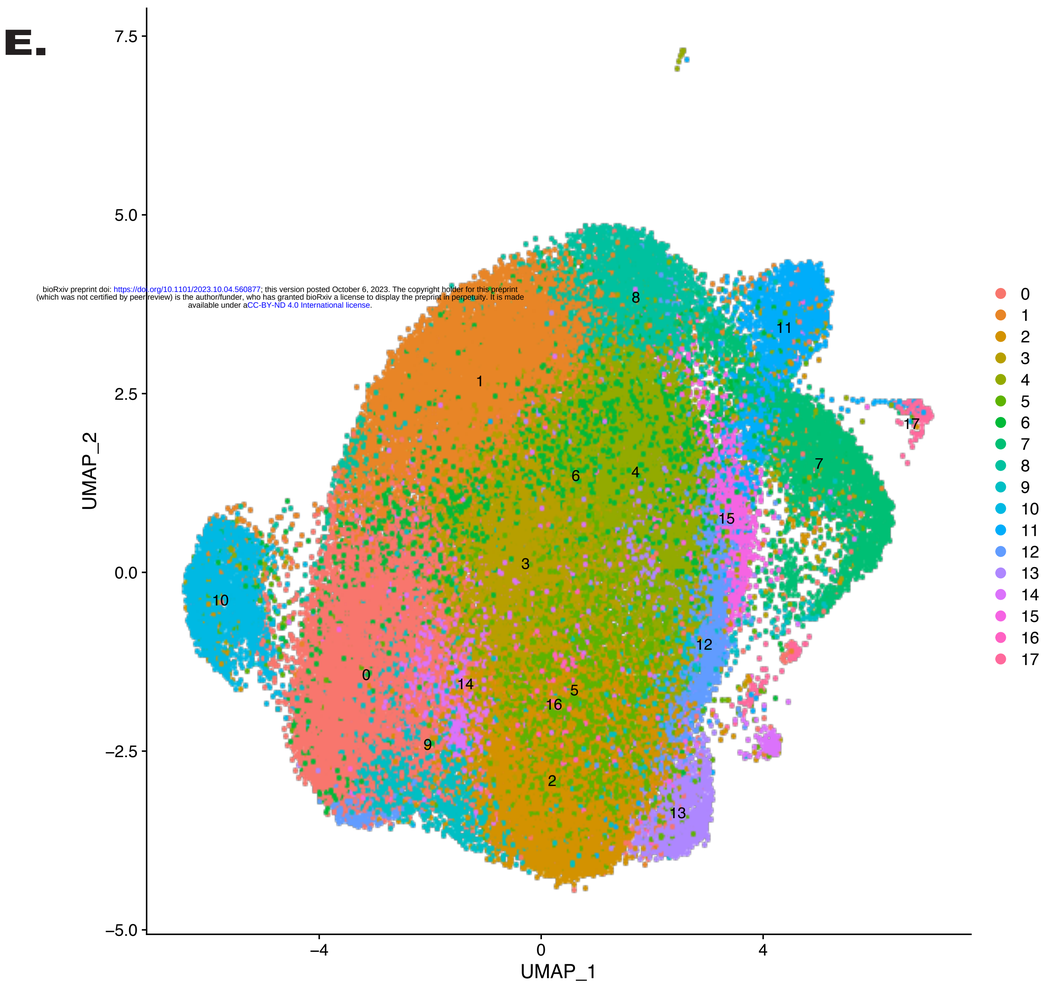

F.

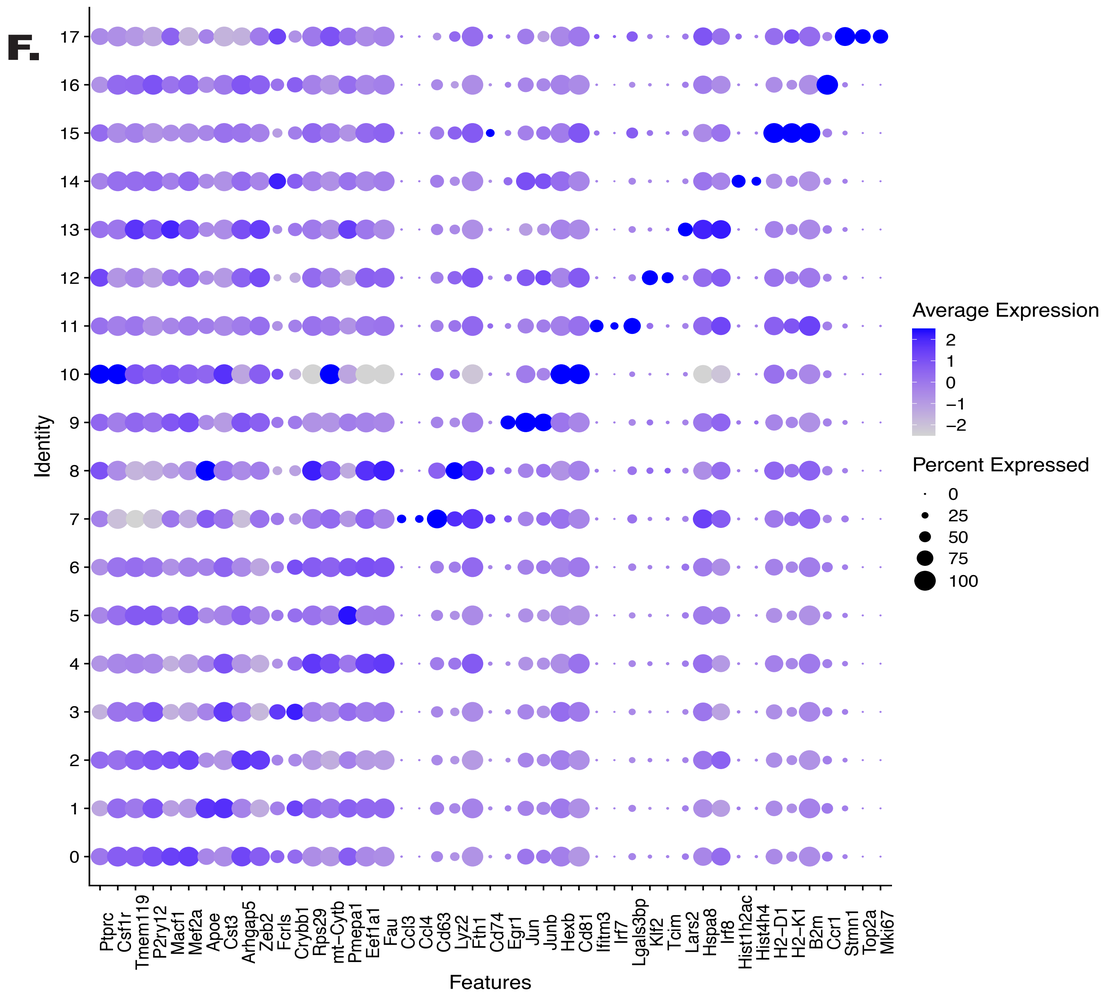

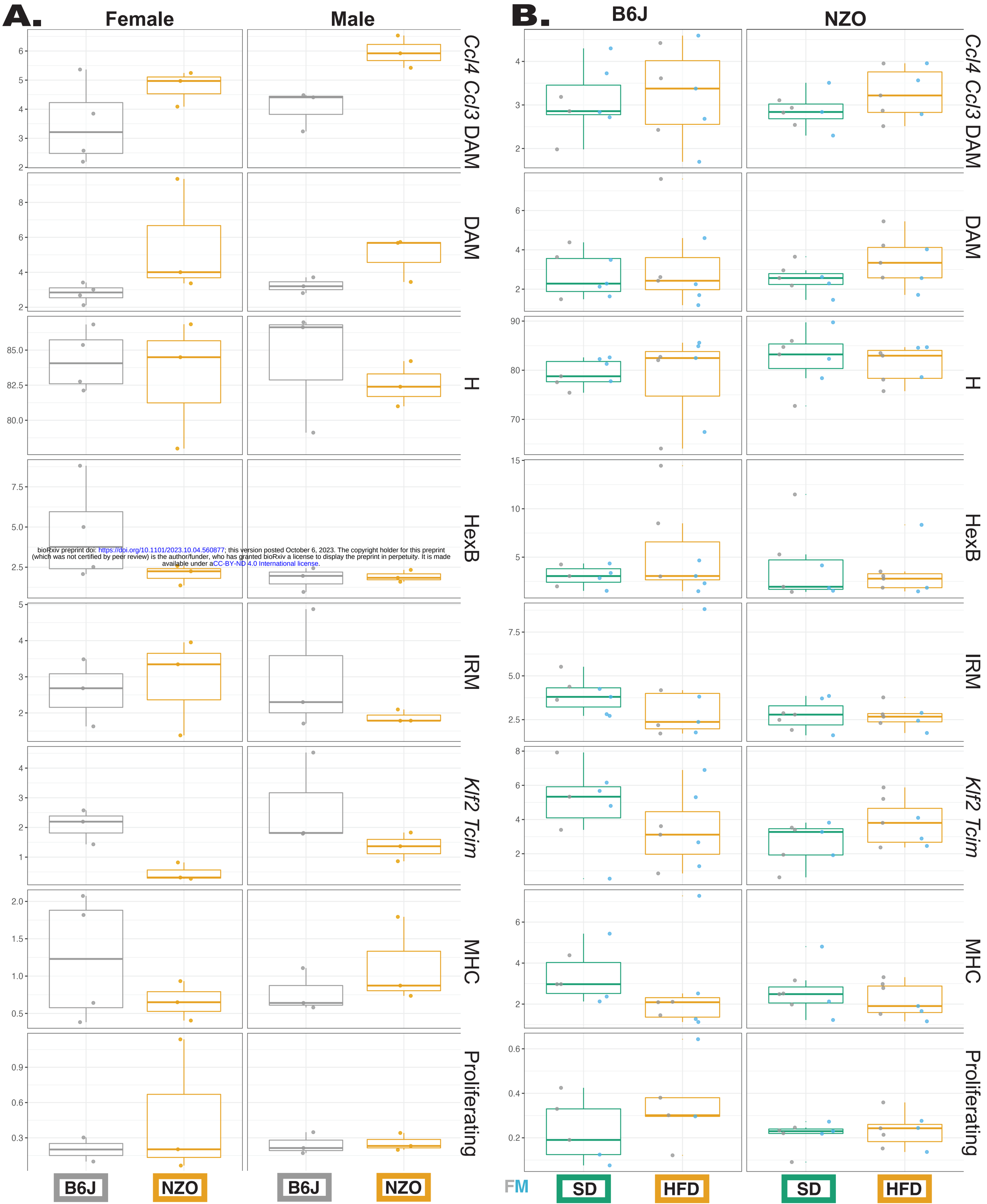

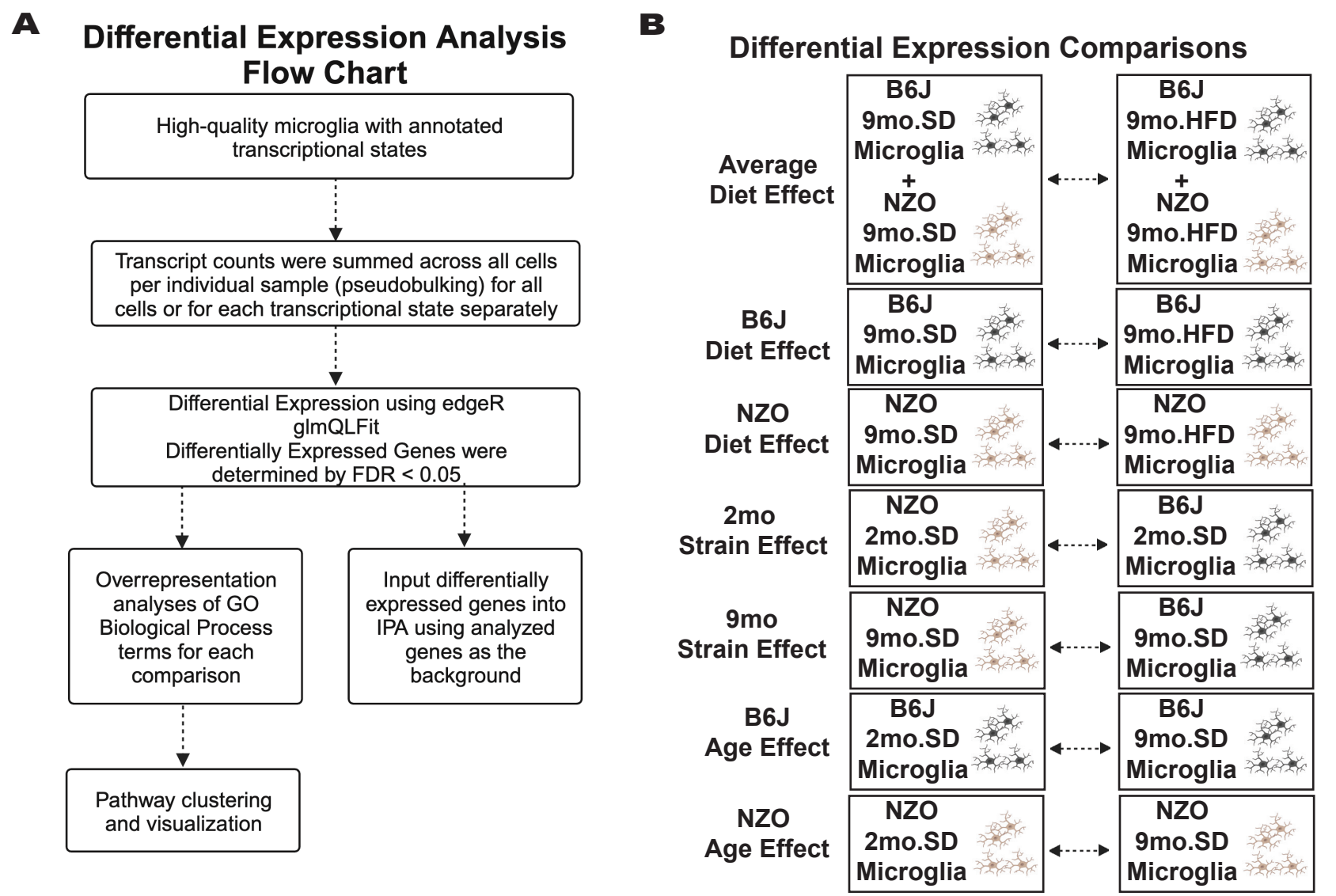
A
Differential Expression Analysis Flow Chart
High-quality microglia with annotated transcriptional states
Transcript counts were summed across all cells per individual sample (pseudobulking) for all cells or for each transcriptional state separately
Differential Expression using edgeR glmQLFit
Differentially Expressed Genes were determined by FDR < 0.05
Overrepresentation analyses of GO Biological Process terms for each comparison
Input differentially expressed genes into IPA using analyzed genes as the background
Pathway clustering and visualization
B
Differential Expression Comparisons
Average Diet Effect
B6J 9mo.SD Microglia + NZO 9mo.SD Microglia
B6J 9mo.HFD Microglia + NZO 9mo.HFD Microglia
B6J Diet Effect
B6J 9mo.SD Microglia
B6J 9mo.HFD Microglia
NZO Diet Effect
NZO 9mo.SD Microglia
NZO 9mo.HFD Microglia
2mo Strain Effect
NZO 2mo.SD Microglia
B6J 2mo.SD Microglia
9mo Strain Effect
NZO 9mo.SD Microglia
B6J 9mo.SD Microglia
B6J Age Effect
B6J 2mo.SD Microglia
B6J 9mo.SD Microglia
NZO Age Effect
NZO 2mo.SD Microglia
NZO 9mo.SD Microglia

A

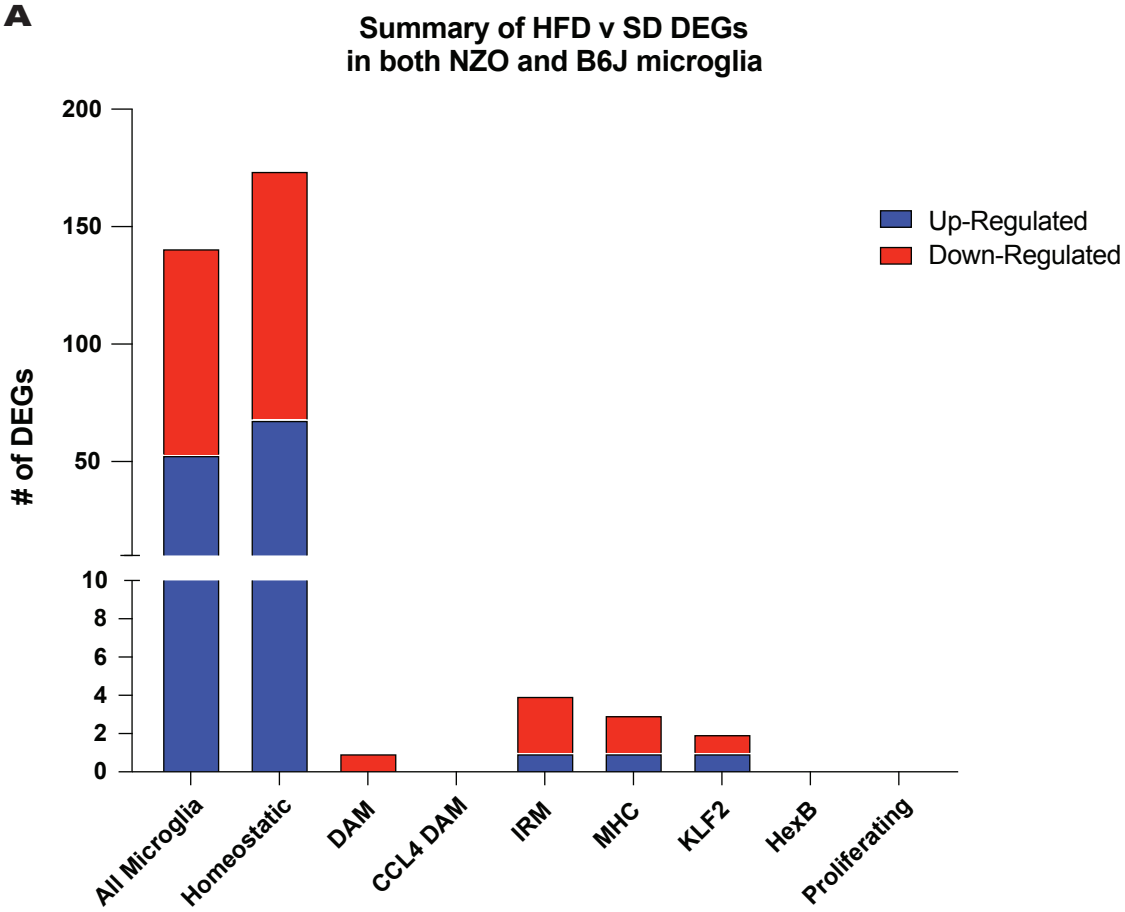
Summary of HFD v SD DEGs
in both NZO and B6J microglia
# of DEGs
200
150
100
50
10
8
6
4
2
0
Up-Regulated
Down-Regulated
All Microglia
Homeostatic
DAM
CCL4 DAM
IRM
MHC
KLF2
HexB
Proliferating

B

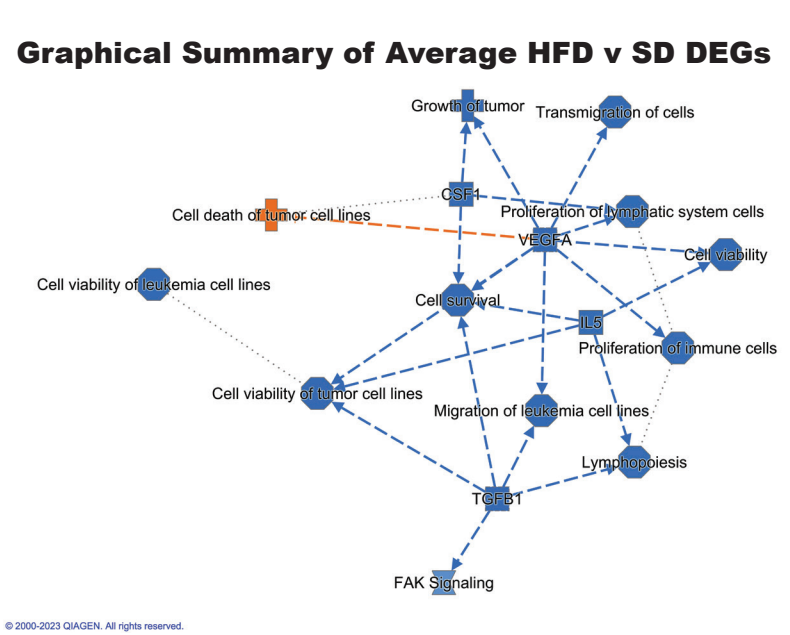
Graphical Summary of Average HFD v SD DEGs
Growth of tumor
Transmigration of cells
CSF1
Cell death of tumor cell lines
Proliferation of lymphatic system cells
VEGFA
Cell viability
Cell viability of leukemia cell lines
Cell survival
IL5
Proliferation of immune cells
Cell viability of tumor cell lines
Migration of leukemia cell lines
Lymphopoiesis
TGFB1
FAK Signaling
© 2000-2023 QIAGEN. All rights reserved.

C

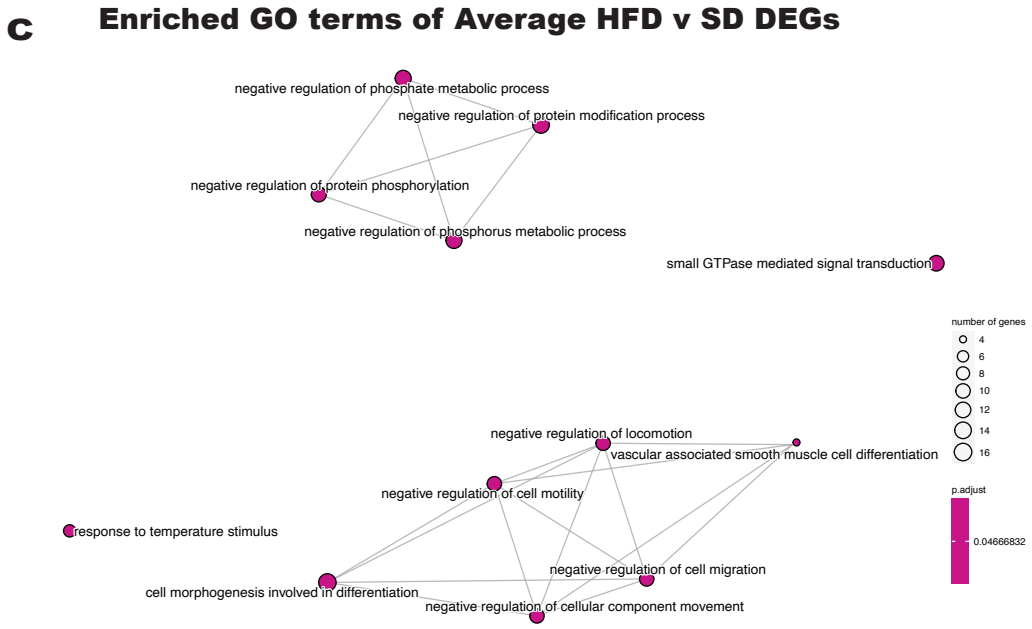
Enriched GO terms of Average HFD v SD DEGs
negative regulation of phosphate metabolic process
negative regulation of protein modification process
negative regulation of protein phosphorylation
negative regulation of phosphorus metabolic process
small GTPase mediated signal transduction
number of genes
4
6
8
10
12
14
16
p.adjust
0.04666832
negative regulation of locomotion
vascular associated smooth muscle cell differentiation
negative regulation of cell motility
response to temperature stimulus
negative regulation of cell migration
cell morphogenesis involved in differentiation
negative regulation of cellular component movement

D

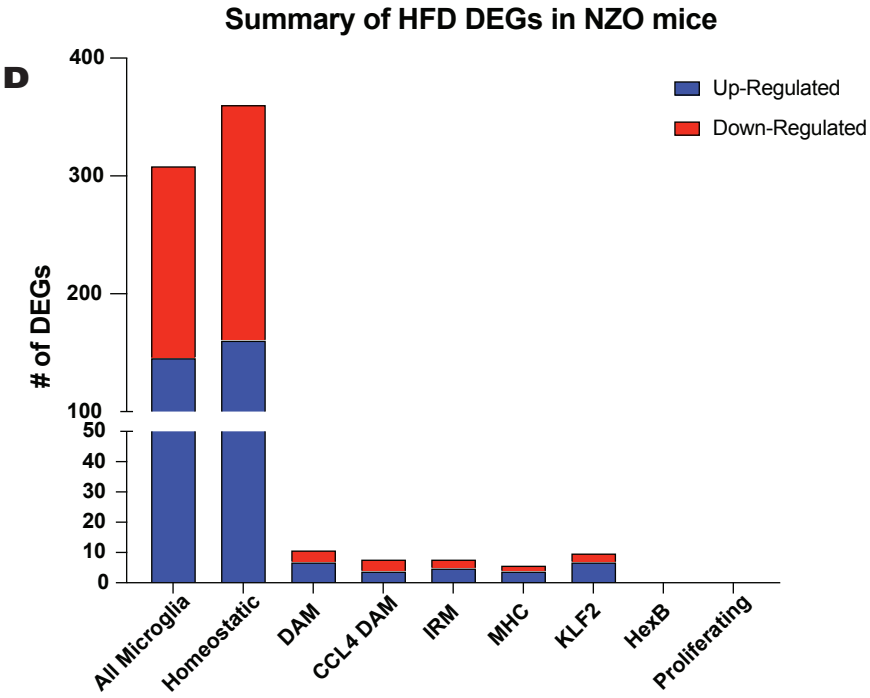
Summary of HFD DEGs in NZO mice
# of DEGs
400
300
200
100
50
40
30
20
10
0
Up-Regulated
Down-Regulated
All Microglia
Homeostatic
DAM
CCL4 DAM
IRM
MHC
KLF2
HexB
Proliferating

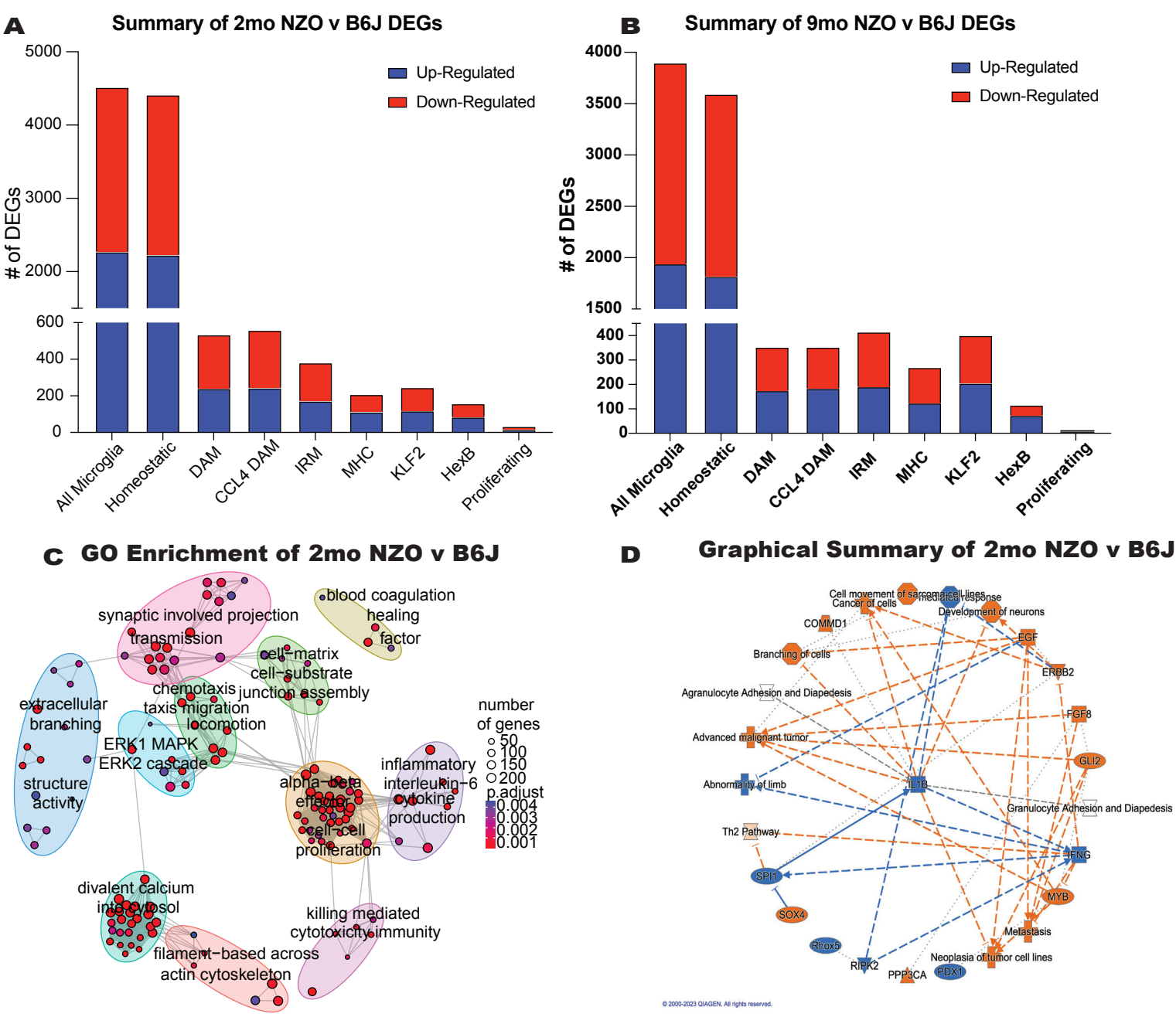
A
Summary of 2mo NZO v B6J DEGs
# of DEGs
Up-Regulated
Down-Regulated
All Microglia
Homeostatic
DAM
CCL4 DAM
IRM
MHC
KLF2
HexB
Proliferating
B
Summary of 9mo NZO v B6J DEGs
# of DEGs
Up-Regulated
Down-Regulated
All Microglia
Homeostatic
DAM
CCL4 DAM
IRM
MHC
KLF2
HexB
Proliferating
C
GO Enrichment of 2mo NZO v B6J
synaptic involved projection
transmission
blood coagulation
healing
factor
cell−matrix
cell−substrate
junction assembly
chemotaxis
taxis migration
locomotion
extracellular
branching
structure
activity
ERK1 MAPK
ERK2 cascade
inflammatory
interleukin−6
cytokine
production
alpha−beta
effector
cell−cell
proliferation
divalent calcium
cytosol
killing mediated
cytotoxicity immunity
filament−based across
actin cytoskeleton
number
of genes
50
100
150
200
p.adjust
0.004
0.003
0.002
0.001
D
Graphical Summary of 2mo NZO v B6J
Cell movement of sarcoma cell lines
Cancer of cells
Immune response
Development of neurons
COMMD1
EGF
Branching of cells
ERBB2
Agranulocyte Adhesion and Diapedesis
FGF8
Advanced malignant tumor
GLI2
Abnormality of limb
IL1B
Granulocyte Adhesion and Diapedesis
Th2 Pathway
IFNG
SPI1
MYB
SOX4
Metastasis
Rhox5
Neoplasia of tumor cell lines
RIPK2
PPP3CA
PDX1
© 2000-2023 QIAGEN. All rights reserved.

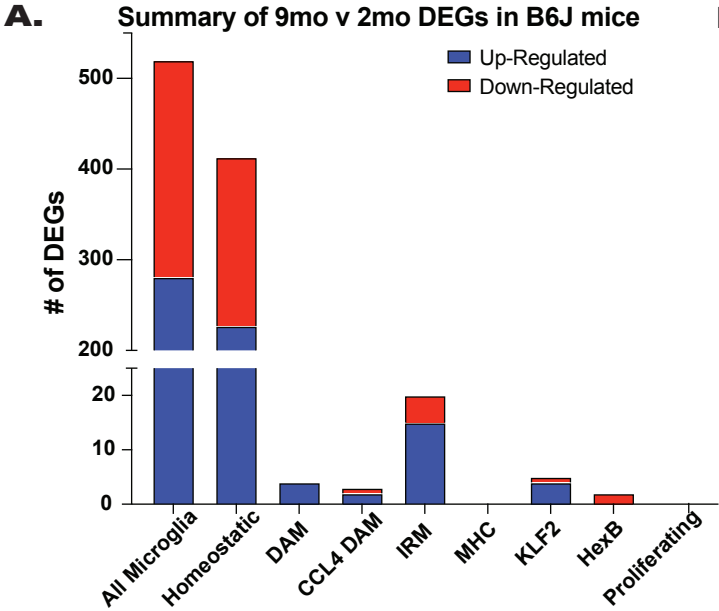
A.
Summary of 9mo v 2mo DEGs in B6J mice
Up-Regulated
Down-Regulated
# of DEGs
500
400
300
200
20
10
0
All Microglia
Homeostatic
DAM
CCL4 DAM
IRM
MHC
KLF2
HexB
Proliferating

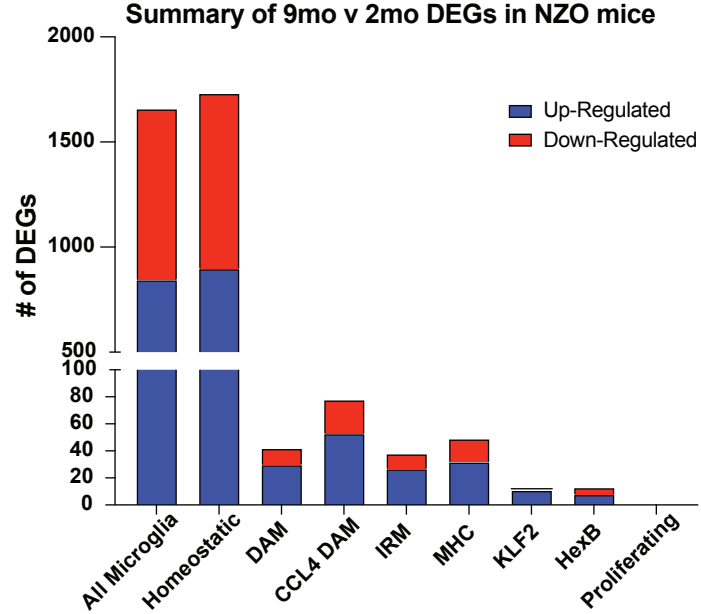
B.
Summary of 9mo v 2mo DEGs in NZO mice
Up-Regulated
Down-Regulated
# of DEGs
2000
1500
1000
500
100
80
60
40
20
0
All Microglia
Homeostatic
DAM
CCL4 DAM
IRM
MHC
KLF2
HexB
Proliferating

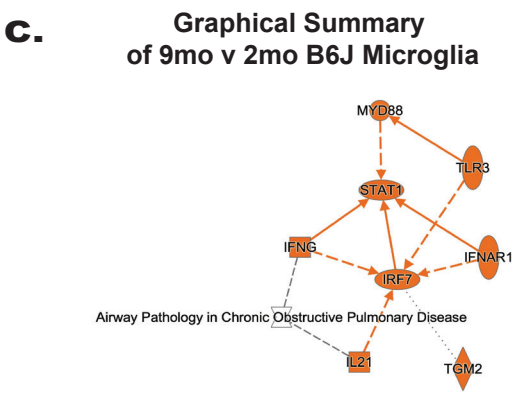
C.
Graphical Summary
of 9mo v 2mo B6J Microglia
MYD88
TLR3
STAT1
IFNG
IFNAR1
IRF7
Airway Pathology in Chronic Obstructive Pulmonary Disease
IL21
TGM2

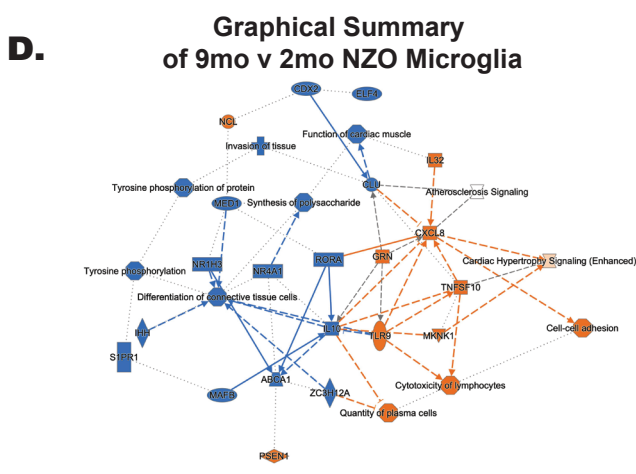
D.
Graphical Summary
of 9mo v 2mo NZO Microglia
CDX2
ELF4
NCL
Function of cardiac muscle
Invasion of tissue
IL32
Tyrosine phosphorylation of protein
CLU
Atherosclerosis Signaling
MEF2
Synthesis of polysaccharide
CXCL8
Tyrosine phosphorylation
NR1H3
NR4A1
RORA
GRN
Cardiac Hypertrophy Signaling (Enhanced)
Differentiation of connective tissue cells
TNFSF10
IL6
IL17
TLR9
MKNK1
Cell-cell adhesion
S1PR1
ABCA1
MAFB
ZC3H12A
Cytotoxicity of lymphocytes
Quantity of plasma cells
PSEN1
© 2000-2023 QIAGEN. All rights reserved.

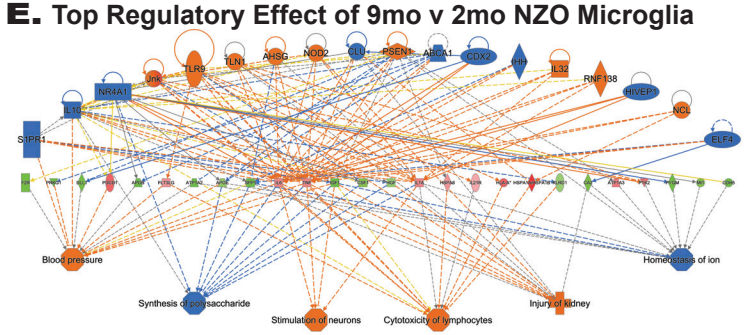
E. Top Regulatory Effect of 9mo v 2mo NZO Microglia
Blood pressure
Homeostasis of ion
Synthesis of polysaccharide
Injury of kidney
Stimulation of neurons
Cytotoxicity of lymphocytes

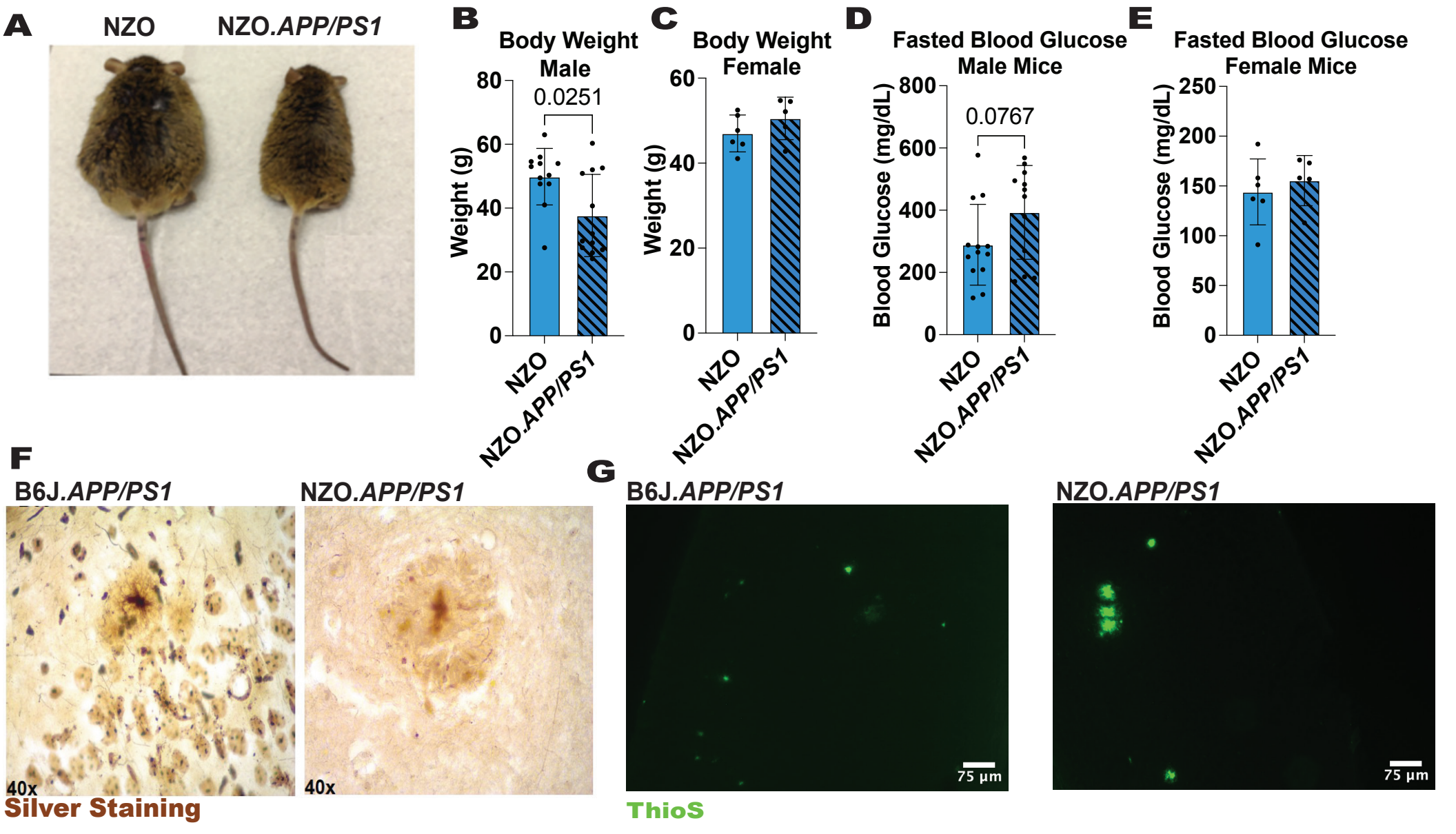
A
NZO
NZO.APP/PS1
B
Body Weight
Male
0.0251
Weight (g)
80
60
40
20
0
NZO
NZO.APP/PS1
C
Body Weight
Female
Weight (g)
60
40
20
0
NZO
NZO.APP/PS1
D
Fasted Blood Glucose
Male Mice
0.0767
Blood Glucose (mg/dL)
800
600
400
200
0
NZO
NZO.APP/PS1
E
Fasted Blood Glucose
Female Mice
Blood Glucose (mg/dL)
250
200
150
100
50
0
NZO
NZO.APP/PS1
F
B6J.APP/PS1
NZO.APP/PS1
40x
40x
Silver Staining
G
B6J.APP/PS1
NZO.APP/PS1
75 µm
75 µm
ThioS